

Bosutinib prevents vascular leakage by reducing focal adhesion turnover and reinforcing junctional integrity

Liza Botros, MD.¹⁻², Manon CA Pronk, PhD.², Jenny Juschten, MD.³, John Liddle⁴, Sofia KSH Morsing⁶, Jaap D van Buul PhD.⁶, Robert H Bates⁴, Pieter R Tuinman MD. PhD.³, Jan SM van Bezu², Stephan Huveneers PhD.⁵, Harm Jan Bogaard MD. PhD.¹, Victor WM van Hinsbergh PhD.², Peter L Hordijk PhD.², Jurjan Aman MD. PhD.¹

¹Amsterdam UMC, Vrije Universiteit Amsterdam, Department of Pulmonology, Amsterdam Cardiovascular Sciences, 1081 BT Amsterdam, The Netherlands.

²Amsterdam UMC, Vrije Universiteit Amsterdam, Department of Physiology, Amsterdam Cardiovascular Sciences, 1081 BT Amsterdam The Netherlands.

³Amsterdam UMC, University of Amsterdam Department of Intensive Care, 1105 AZ Amsterdam The Netherlands.

⁴GlaxoSmithKline, Stevenage, United Kingdom.

⁵Amsterdam UMC, University of Amsterdam, Department of Medical Biochemistry, Amsterdam Cardiovascular Sciences, 1105 AZ Amsterdam, The Netherlands

⁶Molecular Cell Biology Lab at Dept. Molecular Cellular Haemostasis, Sanquin Research and Landsteiner Laboratory, Amsterdam, the Netherlands

Corresponding Author

Jurjan Aman, MD. PhD.

Department of Pulmonology

Amsterdam University Medical Centers, location VUmc De Boelelaan 1117

1081 HV Amsterdam The Netherlands

Tel: +31 20 44 48110 e-mail: j.aman@amsterdamumc.nl

Subject codes: Endothelial barrier function, vascular permeability, focal adhesion, tyrosine kinase inhibitors

Author contributions:

JL, VWMvH, HJB, PH and JA contributed to the conception and design of the study and interpretation of the data. LB, MP, JJ, JB, JL, SM, JvB, RB and SH were responsible for data acquisition and analysis. LB, MP, JJ, VWMvH, SH, HJB, PH, and JA drafted the manuscript. All authors critically revised the manuscript for important intellectual content and gave final approval of the version to be published. All authors are accountable for all aspects of the work.

Summary statement

Combined inhibition of Arg and mitogen-activated protein kinase 4 (MAP4K4) by bosutinib enhances turnover of integrin-based focal adhesions. This provides robust protection against inflammation-induced vascular leakage.

ABSTRACT

Aims: Endothelial barrier dysfunction leads to edema and vascular leak, carrying high morbidity and mortality. Previously, Abl kinase inhibition was shown to protect against vascular leak. Using the distinct inhibitory profiles of clinically available Abl kinase inhibitors, we aimed to provide a mechanistic basis for novel treatment strategies against vascular leakage syndromes.

Methods & Results: Bosutinib most potently protected against inflammation-induced endothelial barrier disruption. In vivo, bosutinib prevented LPS-induced alveolar protein extravasation in an acute lung injury mice model. Mechanistically, Mitogen-activated Protein 4 Kinase 4 (MAP4K4) was identified as important novel mediator of endothelial permeability, which signals via ezrin, radixin and moesin proteins to increase turnover of integrin-based focal adhesions. The combined inhibition of MAP4K4 and Arg by bosutinib preserved adherens junction integrity and reduced turnover of focal adhesions, which synergistically act to stabilize the endothelial barrier during inflammation.

Conclusion: MAP4K4 was identified as important regulator of endothelial barrier integrity, increasing focal adhesion turnover and disruption of cell-cell junctions during inflammation. Inhibiting both Arg and MAP4K4, the clinically available drug bosutinib may form a viable strategy against vascular leakage syndromes.

ABBREVIATIONS

AJ	Adherens Junctions
AKI	Abl Kinase Inhibitor
ARDS	Acute Respiratory Distress Syndrome
Arg	Abl-Related Gene
BALF	Broncho-Alveolar Lavage Fluid
DMSO	Dimethyl Sulfide Oxide
ECIS [®]	Electrical Cell-substrate Impedance Sensing
ECM	Extracellular Matrix
ERM	Ezrin Radixin Moesin
FA	Focal Adhesions
GFP	Green Fluorescent Protein
HRP	Horse Radish Peroxide
HUVEC	Human Umbilical Vein Endothelial Cell
IL-6	Interleukin-6
LPS	Lipopolysaccharide
MAPK	Mitogen-Activated Protein Kinase
MAP4K4	Mitogen-Activated Protein Kinase Kinase Kinase Kinase 4
MLC	Myosin Light Chain
PMVEC	Pulmonary Microvascular Endothelial Cell
TIRF	Total Internal Reflection Fluorescence
TNF α	Tissue Necrosis Factor α
VE-cadherin	Vascular Endothelium Cadherin

INTRODUCTION

The vascular endothelium controls the transport of proteins and solutes from the blood to the tissues (Mehta and Malik, 2006, Komarova et al., 2017). Dysregulation of the endothelial barrier leads to capillary leakage and edema as seen in pathological conditions such as acute respiratory distress syndrome (ARDS) and sepsis (Lee and Slutsky, 2010, Komarova et al., 2017). Inflammatory mediators open endothelial cell junctions, enhancing vascular permeability (Wessel et al., 2014). Despite increased understanding of endothelial barrier regulation at the molecular level (Filewod and Lee, 2019), only supportive care with oxygen supplementation and lung-protective ventilation are available, but do not target the underlying inflammation-induced structural defects in the endothelium (Lee and Slutsky, 2010, Matthay et al., 2019).

Adherens junctions (AJ) comprise transmembrane proteins that form dynamic interactions between adjacent cells and play an important role in maintaining the integrity of the vascular endothelial monolayer and in the regulation of its barrier function (Dejana and Giampietro, 2012, Gavard, 2013). The main AJ protein is vascular-endothelial (VE) cadherin, a single span transmembrane, homotypic adhesion molecule which connects intracellularly to the cortical F-actin cytoskeleton (Dejana and Giampietro, 2012). In the presence of pro-inflammatory stimuli, intracellular signalling leads to phosphorylation, destabilization and internalization of VE-cadherin (Gavard, 2013). In parallel, activation of RhoGTPases induces actomyosin based contraction, following the phosphorylation of myosin light chain (MLC), which lead to contractile stress fibres, exertion of force on the junctional complexes and finally retraction of the cell membrane (Mehta and Malik, 2006, Huveneers et al., 2012).

We have previously demonstrated that the Abl kinase inhibitor (AKI) imatinib reverses pulmonary edema (Aman et al., 2013) and protects against endothelial barrier disruption by inhibition of Abl-related gene (Arg) (Aman et al., 2012). The inhibition of Arg resulted both in enhanced cell–cell interactions and enhanced cell–matrix adhesion. Mechanistically, we showed that imatinib-mediated inhibition of Arg increased the activity of Rac1 and the stabilization of peripheral, β 1-integrin containing, focal adhesions (FA). FA are multi-protein structures that link the

cytoskeleton to the extracellular matrix (ECM) (Hynes, 2002). Within FA, integrins play a pivotal role both in cell-matrix adhesion and in bidirectional signaling across the plasma membrane (Shattil et al., 2010). Similar to cadherins, the intracellular domains of integrins are dynamically connected to the actin cytoskeleton through a large variety of adapter and signaling proteins. As a result, integrin stability and adhesive function is subject to regulation by signaling from within the cell ('inside-out' signaling). Conversely, integrins probe the extracellular environment where their adhesive interactions with the ECM trigger subsequent intracellular ('outside-in') signaling (Shattil et al., 2010, Hynes, 2002).

Integrins are essential for endothelial barrier stability, cell migration and proliferation (Shattil et al., 2010, Yamamoto et al., 2015, Song et al., 2017) and there is growing evidence for a role of FA and β 1-integrins in blood vessel stability and barrier function (Pulous et al., 2019, Hakanpaa et al., 2018, Yamamoto et al., 2015). Integrin-containing FA have shown to stabilize and localize VE-cadherin at cell-cell junctions (Pulous et al., 2019, Yamamoto et al., 2015), although the underlying mechanism remains unclear. The involvement of integrins in endothelial barrier regulation is diverse and is dependent on the availability of different integrin subtypes and their cellular distribution (Su et al., 2012, Su et al., 2007, Hakanpaa et al., 2018).

Next generation AKIs have been developed to treat imatinib-resistant forms of chronic myeloid leukemia (Khoury et al., 2012) that show different kinase inhibition and safety profiles. We hypothesized that inhibition of a favorable combination of kinases (as provided by next generation AKIs), provides greater potential for the treatment of vascular leakage syndromes. In the current study, we made use of the distinct inhibitory profiles of clinically available AKIs to provide a mechanistic basis for novel treatment strategies against vascular leakage syndromes (Gover-Proaktor et al., 2018). We identified the clinically available AKI bosutinib as robust protector of vascular permeability both in vitro and in vivo, which exerts its protective effect through combined inhibition of Arg and Mitogen-activated Protein Kinase 4 (MAP4K4).

RESULTS

Bosutinib provides full protection against thrombin-induced endothelial barrier disruption

Previously, we identified the kinase inhibitor imatinib as a compound which protects against agonist-induced loss of barrier function (Aman et al., 2012). In search for novel, more effective barrier-protecting compounds, we tested three generations of Abl-kinase inhibitors on endothelial barrier function in HUVECs (Fig 1A,B, Fig S 1A,B). In these studies, we challenged stable endothelial monolayers with the protease thrombin, which represents a well-established model for inflammation induced loss of endothelial integrity. Similar to other G-protein-coupled receptor agonists, the loss of barrier function induced by thrombin is acute and reversible (Fig S1B). Our screen showed that the synthetic quinolone derivate bosutinib demonstrated the strongest protection to thrombin-challenged loss of endothelial barrier function. This was observed both in macromolecule passage assays (Fig. 1A&S1A) and in transendothelial electrical resistance assays (Fig. 1B&S1B). Validation experiments further confirmed that bosutinib increased basal barrier function, (Fig. S1C), and that bosutinib protected against thrombin and histamine-induced endothelial barrier disruption (Fig. 1C,D&S1D) at an optimal concentration of 1 μ M (Fig. S1E,F). Cell viability assays showed no cell toxicity at this concentration (Fig. S1G). Similar protective effects were observed in PMVECs (Fig. 1E) showing that barrier protection by bosutinib is neither agonist nor endothelial cell-type specific. These experiments demonstrate a strong protective effect of bosutinib against inflammation-induced endothelial barrier loss.

Subsequent immunofluorescent studies showed that bosutinib in both PMVECs and HUVECs protected against thrombin-induced intercellular gap formation,(Fig. 1F,G; S1H,I) and increased VE-cadherin intensity at cell-cell junctions (Fig. 1F,H; Fig S1H,J). Moreover, bosutinib increased the number of β 1-integrin-positive FAs (Fig. 1F, I, Fig S1H,K). Bosutinib did not reduce F-actin stress fiber formation or Ser18/Thr19-phosphorylation of MLC (Fig. S1L), indicating that bosutinib does not inhibit actomyosin contractility. Total, VE-cadherin or vinculin levels did not change after bosutinib treatment in Western blot (Fig. S1M-N). These results suggest

that bosutinib protects against endothelial barrier disruption by enhancing VE-cadherin-containing adherens junctions and reinforcing β 1-integrin-containing FAs.

Inhibition of Mitogen-activated protein kinase 4 (MAP4K4) by bosutinib stabilizes endothelial barrier function

Our previous studies showed that imatinib prevents endothelial barrier dysfunction and edema via inhibition of Arg (Aman et al., 2012). As bosutinib had stronger barrier-protective effects than imatinib (Fig 1A,B), we hypothesized that combined inhibition of multiple kinases favors endothelial barrier preservation under inflammatory conditions. To understand which kinases could be involved, bosutinib and imatinib were profiled by measuring the inhibitory activity against 369 kinases at a single concentration in competition binding assays. Thresholds for kinase inhibition of $\geq 75\%$ at 10nM bosutinib and $\leq 50\%$ at 10 μ M imatinib were chosen to select candidate kinases that may account for the differential effects of these two inhibitors on endothelial barrier function (Fig 2A). Interestingly, bosutinib showed specificity against several mitogen-activated protein family of kinases (MAP4K4, MAP4K5, MAP4K6, MAP4K7). Since bosutinib showed highest specific kinase inhibition against MAP4K5, siRNA-mediated knockdown of MAP4K5 was tested in ECIS and compared to knockdown of MAP4K4, a kinase known to regulate focal adhesion and barrier function (Yue et al., 2014, Vitorino et al., 2015, Roth Flach et al., 2015). siRNA-mediated knockdown of MAP4K4 resulted in specific and efficient ($>80\%$) depletion of MAP4K4 (Fig S2A,B). To our surprise, depletion of MAP4K4, but not MAP4K5, significantly attenuated thrombin-induced barrier disruption (Fig. 2B& S2C). Simultaneous knockdown of both MAP4K4 and MAP4K5 did not further improve barrier protection (Fig. 2B,C). Different siRNAs for MAP4K4 displayed a similar degree protective effect during thrombin stimulation (Fig. S2D).

As prolonged knockdown may result in compensatory upregulation of redundant pathways, we evaluated the effect of a pharmacological MAP4K4 inhibitor (PF-6260933) that inhibits the trio of MAP4K4, 6 and 7 (Ammirati et al., 2015, Roth Flach et al., 2015). Treatment with PF-6260933 increased basal monolayer resistance and significantly attenuated the thrombin-induced loss of barrier function (Fig. 2C). MAP4K4 shares greater than 90% amino acid identity with MINK/MAP4K6 and TNIK/MAP4K7 (Chuang et al., 2016) and redundancy and overlapping functions

have been described for these kinases (Baumgartner et al., 2006, Chuang et al., 2016). Knockdown of MAP4K6 and 7 did not improve endothelial barrier function and combined knockdown of the trio MAP4K4/6/7 gave similar results compared to siMAP4K4 alone (Fig. 2D, S2E). Knockdown efficiency and specificity is depicted in Fig. S2A&F-H, showing that MAP4K5 had some cross-reactivity with MAP4K6/7.

As Arg is inhibited by both bosutinib and imatinib, we hypothesized that combined inhibition of Arg and MAP4K family of kinases, results in a similar protective effect as bosutinib treatment. To test this, macromolecule passage was measured under basal conditions, showing significant reduction of macromolecule passage in siMAP4K4 (Fig. S2I), in line with the barrier stabilizing effect of bosutinib (Fig. 1C). Knockdown of MAP4K4 either alone or combined with the loss of Arg effectively reduced thrombin-induced HRP passage, although this effect did not mimic the protective effect of bosutinib completely (Fig. S2J). Likely, acute kinase inhibition by bosutinib is more effective in barrier protection as compared to the siRNA-mediated loss of cognate kinase expression quantified only after 72 hrs.

Notably, knockdown of Arg combined with PF-6260933 completely mimicked the positive effect of bosutinib on basal endothelial barrier function as well as thrombin-induced loss of integrity (Fig. 2D&S2K,I). Together, these data show that combined kinase inhibition of Arg and MAP4K4 can account for the protective effects of bosutinib on endothelial barrier function.

To evaluate the effect of MAP4K4 on cell-cell junctions and cell-ECM interaction, immunostaining for VE-cadherin, active β 1-integrin and F-actin was performed after treatment with siMAP4K4, siArg and PF-6260933 (Fig. 3A). VE-cadherin intensity was unaltered under basal conditions (Fig S3A,B). After thrombin stimulation, MAP4K4 knockdown or its inhibition completely prevented intercellular gap formation (Fig. 3A,B). In line with this, thrombin-induced loss of VE-cadherin intensity at the cell periphery was fully preserved after PF-6260933 treatment (Fig. 3C). Similar to bosutinib treatment, the number of FAs increased after inhibition or loss of MAP4K4 under basal conditions (Fig S3C) as well as in thrombin stimulated cells (Fig 3D). Peripheral focal adhesions were increased with bosutinib treatment, PF-6260933, siMAP4K4 and siArg with PF-6260933 (Fig 3E). Since the total number

of FA also increased, the ratio remained unaltered in all conditions except bosutinib treatment (Fig. 3F).

In line with the effects of bosutinib on the F-actin cytoskeleton (Fig S1H), stress fiber formation was not affected by the loss or inhibition of Arg or MAP4K4 (Fig. S3A), indicating that increased acto-myosin-based contraction is not sufficient for intercellular gap formation. Together, these data provide further evidence that MAP4K4 and Arg both negatively regulate the stabilization of FAs and adherens junctions, and that combined loss or inhibition of these kinases might recapitulate the strong barrier protective effects of bosutinib.

MAP4K4 increases focal adhesion turnover

As recent studies pointed to a role for β 1-integrin activation in maintaining VE-cadherin at AJs (Yamamoto et al., 2015, Pulous et al., 2019, Hakanpaa et al., 2018) and bosutinib enhanced β 1-integrin localization in peripheral FAs (see Fig. 1F,I & Fig. 3D-F), we tested if MAP4K4 inhibition may have an additional effect via FA reorganization. The involvement of MAP4K4 in FA dynamics was analyzed using live-cell imaging of primary human endothelial cells expressing GFP-vinculin (Movie 1-3, Online Supplement). Time lapse images of GFP-vinculin expressing endothelial cells show basal FA dynamics after treatment with bosutinib or PF-6260933, followed by thrombin stimulation, in line with the data in Fig. 3B. Both bosutinib and PF-6260933 increased the abundance of FAs in unstimulated and in thrombin-treated cells. (Fig. 4A). We next quantified FA turnover, which showed that FA assembly and disassembly were decreased by bosutinib and PF-6260933 under basal and thrombin-stimulated conditions (Fig. 4B,C). This results in increased FA lifetime (Fig. 4D). In further support of a FA-stabilizing effect, bosutinib increased cell spreading as measured by ECIS (Fig. S3D-E) and by microscopy (Fig. 4E) without changing F-actin levels or MLC phosphorylation (Fig. S1L).

Because MAP4K4 inhibition induced stabilization of both FA and AJ, we evaluated whether the observed FA stabilization contributes to AJ stabilization and endothelial barrier protection by bosutinib. We therefore used peptides that block integrin adhesive function (GRGDSP; GRGDNP) to evaluate whether bosutinib still protects the endothelial barrier in the absence of functional integrins and FA. GRGDSP is described to bind α v β 5 and α 5 β 1 but preferential binding to α v β 3.

GRGDNP also blocks adhesion by $\alpha v\beta 3$ and $\alpha 5\beta 1$ with similar specificity but preferential binding to $\alpha 5\beta 1$ (Kapp et al., 2017). As measured by transendothelial resistance, the simultaneous addition of GRGDSP and/or GRGDNP induced a loss of endothelial integrity in a concentration-dependent manner (Fig. S3F). No differences were observed between the different peptides when tested individually (Fig. S3G-H). Using an integrin- $\beta 1$ blocking peptides in a low concentration at which the basal barrier function was not compromised ($450\mu\text{M}$), we found that bosutinib no longer rescued the thrombin-induced drop in barrier function (Fig. 4F,G & S3I). These results indicate that functional integrins are required for the barrier-protective effects of bosutinib and help to stabilize the endothelial barrier during thrombin-induced actomyosin contraction.

The MAP4K4-ERM pathway drives focal adhesion turnover during endothelial barrier disruption

Since MAP4K4 enhances FA turnover via phosphorylation of the ezrin, radixin and moesin (ERM) group of proteins (Vitorino et al., 2015), and since MAP4K4 directly binds the N-terminus of moesin (Baumgartner et al., 2006), we hypothesized that MAP4K4 signals via ERM proteins to stabilize FAs and barrier function. In immunofluorescence studies, siMAP4K4 or PF-6260933 reduced junctional localization and intensity of phosphorylated ERM (Fig. 5A,B). Moreover, bosutinib treatment significantly decreased total phosphorylation of ERM proteins in western blot upon thrombin stimulation at several time points (Fig. 5C). This was not seen in cells treated with siMAP4K4, siArg or PF-6260933 (Fig. 5D&S4A)).

To test whether ERM proteins act downstream MAP4K4 during thrombin-induced barrier disruption, we compared the effect of silencing ezrin and moesin (siEzrin+siMoesin), both expressed in endothelial cells (Adyshev et al., 2013) with loss of MAP4K4 on thrombin-induced barrier disruption (see Fig. S4B for knockdown efficiency). Although siMAP4K4 and siEzrin+siMoesin attenuated the thrombin-induced drop in endothelial barrier function to a similar extent, combined siEzrin+siMoesin and siMAP4K4 had an additive protective effect (Fig. 5E&S4C). This can be explained by the fact that we observed restoration of VE-cadherin junctional intensity after thrombin stimulation in siEzrin+siMoesin treated cells, but not in siMAP4K4 treated cells (Fig. 5F,G). Furthermore, siMAP4K4 and

siEzrin+siMoesin increased the number of FA to a similar extent, whereas the triple knockdown had no additive effect (Fig. 5H). Together, these data indicate that ERM proteins act downstream of MAP4K4 in stabilization of β 1-integrin-based FA, whereas ERM proteins stabilize junctional VE-cadherin in a MAP4K4-independent manner.

Bosutinib treatment attenuates LPS-induced pulmonary vascular leakage

Bosutinib is currently in clinical use for the treatment of chronic myeloid leukemia (Khoury et al., 2012, Kong et al., 2017). Repurposing bosutinib for prevention of vascular damage and edema would have large clinical benefit. We therefore tested the vascular barrier protective effects of bosutinib in a clinically relevant mouse model for pulmonary vascular leakage. Lung inflammation and edema were induced via intranasal administration of LPS in mice concomitantly treated with bosutinib (20 mg/kg) or saline (control) injection as previously described (Tuinman et al., 2013) (Fig. 6A). Lung vascular leakage, measured by the lung weight/body weight ratio and protein concentration in BALF, was significantly increased in the LPS treated animals and this effect was prevented by bosutinib (Fig. 6B,C). As an additional measure of vascular leakage, 0.5% Evans Blue was administered intravenously five hours after the induction of lung injury, and organs were harvested one hour after Evans Blue administration. Evans Blue extravasation was significantly increased in lungs and kidneys of LPS-treated mice, an effect that was prevented in bosutinib-treated mice (Fig. S5A-C).

Inflammation, measured by total cell count, percentage neutrophils together with IL-6 levels in BALF were markedly increased after LPS administration and significantly attenuated by bosutinib treatment (Fig. 6D-F), although active trans-endothelial neutrophil migration over pulmonary endothelial cells was not affected by bosutinib (Fig. S5F). TNF- α concentration in BALF was increased after LPS exposure, however, no significant reduction was observed with bosutinib treatment (Fig. S5D). A systemic inflammatory cytokine response measured by circulating IL-6 in plasma was not observed (Fig. S5E). As an additional measure of direct lung injury, the LPS-treated mice showed a significantly higher histopathology score in endothelialitis, edema, interstitial inflammation and hemorrhage in the lungs, whereas bosutinib significantly reduced edema and hemorrhage scores (Fig. 6G). These data

demonstrate that repurposing the clinically available drug bosutinib, effectively reduces inflammation-induced lung vascular leakage.

DISCUSSION

While the molecular basis of endothelial integrity is extensively studied, compounds that provide effective protection against vascular leak, strongly associated with inflammatory disease, remain to be identified. Here we show that the AKI bosutinib provides full protection against agonist-induced endothelial- and vascular permeability in vitro and in vivo. We identified MAP4K4 as an important regulator of endothelial barrier function, contributing to adherens junction dissociation and signaling via ERM to increase FA turnover, with subsequent cell retraction and barrier disruption (Fig. 7). Our data support a model in which the turnover of peripheral, β 1-integrin containing FAs contributes to the loss of VE-cadherin mediated cell-cell contact (Fig. 7) (Pulous et al., 2019, Pulous and Petrich, 2019). While we previously showed that the first generation AKI imatinib provides partial protection from vascular leak by inhibiting Arg, bosutinib is more effective due to its additional effect on MAP4K4, a kinase only moderately targeted by imatinib (Fig 2A).

Identification of MAP4K4 as regulator of endothelial barrier function

The regulation and function of individual serine/threonine MAP4K family of kinases is largely unknown, although MAP4K4 has repeatedly emerged as regulator of cell migration, adhesion and FA stabilization (Yue et al., 2014, Huang et al., 2004, Tripolitsioti et al., 2018, Machida et al., 2004). MAP4K4 activation by TNF α regulates important inflammatory responses including cytokine production as well as atherosclerosis and insulin resistance (Ammirati et al., 2015, Roth Flach et al., 2015, Huang et al., 2014). Divergent findings regarding a role for MAP4K4 in endothelial barrier function have been reported. Vitorino et al found no role for MAP4K4 in basal endothelial permeability using siRNA-mediated knockdown. On the other hand, others report that depletion of MAP4K4 increased basal barrier resistance (Pannekoek et al., 2013) and macromolecule permeability reduced in MAP4K4-silenced monolayers basally, and after TNF- α -mediated inflammation in vitro (Roth Flach et al., 2015). A role for MAP4K4 for barrier function has been suggested by the observations that inhibition of MAP4K4 reduces cholesterol accumulation in aorta of mice and knockdown of MAP4K4 increased basal endothelial barrier function (Roth

Flach et al., 2015, Pannekoek et al., 2013). Family members of the serine/threonine MAP4K4 kinase family MAP4K6 and MAP4K7 share a common function in regulating cell shape and migration and show greater than 90% amino acid identity (Baumgartner et al., 2006). Despite this structural similarity only knockdown of MAP4K4, but not 6 and 7 protected against endothelial barrier disruption during inflammation.

Focal adhesion distribution by bosutinib and MAP4K4 is mediated by ERM

We observed that bosutinib and MAP4K4 inhibition stabilized FA dynamics, leading to increased spreading of endothelial cells to the ECM. Since we found imatinib to increase predominantly peripheral FA through Arg inhibition (Aman et al., 2012, Rizzo et al., 2015), we propose that bosutinib exerts an additional effect on FA dynamics by increasing β 1 integrin and FA stability and longevity through MAP4K4 inhibition. Indeed, loss of MAP4K4 and moesin increased the number of both central and peripheral FA (Vitorino et al., 2015). Moesin is the most abundant ERM protein in endothelial cells and the individual ERM proteins show functional redundancy (Adyshev et al., 2013, Fehon et al., 2010). ERM proteins control cell shape through crosslinking the actin cytoskeleton to the plasma membrane (Tachibana et al., 2015, Baumgartner et al., 2006, Adyshev et al., 2013) and phosphorylation of ERM after thrombin stimulation induces its translocation to the cell periphery, modulating AJ integrity and promoting gap formation (Adyshev et al., 2013, Amsellem et al., 2014). pERM were previously also detected in endothelial retraction fibers, linking ERM-phosphorylation to the induction of contraction (Vitorino et al., 2015). In line with these observations, the present study demonstrates that ERM proteins act downstream of MAP4K4 to regulate β 1 integrin activity and FA turnover during inflammation. As MAP4K4 inhibition increased cell adhesion and spreading, the MAP4K4/ERM pathway appears as an important mediator of decreased cell-ECM binding of endothelial cells under inflammatory conditions, although we cannot exclude a role for ERM protein in endothelial barrier regulation independent from MAP4K4.

Interaction between focal adhesions and adherens junctions in endothelial barrier regulation

The protective effects of bosutinib were paralleled by improvement of AJ integrity and FA stability. Whereas the contribution of the AJ to endothelial barrier integrity is undisputed, the functional role of FA, and specifically integrins, is more controversial. We showed that peptides blocking the adhesive function of integrins $\alpha v\beta 5$, $\alpha 5\beta 1$ and $\alpha v\beta 3$ counteracted the protective effect of bosutinib, indicating that FAs are functionally involved in endothelial barrier regulation and required for a functional barrier. It is known that $\beta 1$ -integrin interacts directly with talin (Giancotti, 2000) and that $\beta 1$ -integrins stabilize cell-cell contacts (Yamamoto et al., 2015, Pulous et al., 2019, Song et al., 2017). Although it is reported that integrin engagement leads to disruption of VE-cadherin containing AJ via the activation of Src kinase (Wang et al., 2006) and that $\beta 1$ -integrin-inhibiting antibodies decrease LPS-induced vascular leakage in murine endotoxemia (Hakanpaa et al., 2018), our data demonstrate that bosutinib decreases FA turnover and enhance cell adhesion to impair cell retraction, even in the presence of intact acto-myosin contraction. Although previous studies have shown that intact FA are essential for a mature endothelial barrier (Song et al., 2017, Pulous et al., 2019, Yamamoto et al., 2015) the present study is the first to demonstrate that active regulation of FA turnover contributes to the hyperpermeability response in vitro and in vivo. Inhibition of Arg and MAP4K4 simultaneously with ERM-mediated reinforcement of the AJ, leads to barrier stabilization. This mechanism aligns well with the suggestion in previous studies that peripheral FA reinforce AJ integrity (Hakanpaa et al., 2018, Pulous et al., 2019).

Perspective

Bosutinib attenuated vascular leakage, protein extravasation and inflammation in a murine acute lung injury model, in line with previous research on virus induced vascular leakage in human pulmonary endothelial cells (Gorbunova et al., 2011) and recovery of lung inflammation in an animal model for silicosis (Carneiro et al., 2017). In addition, in our study LPS and bosutinib were administered simultaneously preventing the development of lung edema. Active neutrophil migration remained unchanged in vitro, therefore we could not exclude a direct effect of bosutinib on neutrophil migration. As a clinically available drug, bosutinib is orally administered

and well tolerated (Cortes et al.), with milder cardiac hypertrophy and fewer vascular adverse events compared to several other AKIs (Heyen et al., 2013, Gover-Proaktor et al., 2018). Moreover, only low-grade gastrointestinal toxicity is reported after bosutinib treatment (Kong et al., 2017). Based on these drug characteristics, the fact that bosutinib inhibits endothelial MAP4K4 during inflammation, and the protective effects of bosutinib on vascular endothelial integrity identified in this study, repurposing bosutinib as novel treatment for clinical syndromes associated with vascular leak is a suitable option.

Conclusion

During inflammation, Arg and MAP4K4 signal to increase turnover of integrin-based peripheral FAs, which is required for the loss of VE-cadherin mediated cell-cell contact. This study identifies MAP4K4/ERM signaling as important pathway that mediates stimulus induced FA dissolution and adherens junction dissociation. Since the clinically available drug bosutinib inhibits both Arg and MAP4K4/ERM signaling, bosutinib may be a viable strategy against vascular leakage.

METHODS AND MATERIALS

Reagents, antibodies and siRNAs

For all experiments bosutinib was purchased from Selleck chemicals (s104) and dissolved in dimethylsulphoxide (DMSO) in a concentration of 1 μ M. Imatinib (free base) was purchased from ChemieTek (Indianapolis, IN) and dissolved in DMSO in a concentration of 10 μ M. All tyrosine kinases used in the screen were provided by GlaxoSmithKline (GSK, Stevenage, UK) and used in their optimal concentration: GNF2 10 μ M, Nilotinib 10 μ M, Nintedanib 1 μ M, Erlotinib 10 μ M and Dasatinib 0.1 μ M, as determined by concentration series in ECIS (data not shown). PF-6260933 (Selleckem) was dissolved in sterile water in a concentration of 3 μ M.

The following antibodies were used: α -MAP4K4(HGK, #3485 1:1000), α -VE-cadherin XP (D87F2,#2500 1:200-1000), α -phospho-Ezrin(Thr567)/Radixin(Thr564) /Moesin(Thr558) (#3141S 1:500-1000), α -Ezrin/Radixin/Moesin (#3142 1:500-1000),

pMLC (#3671 1:2000), α -P44/42 MAP Kinase (ERK)(#9102 1:2000) vinculin (#4650 1:5000) all Cell Signaling, α -VE-cadherin (SC-6458, Santa Cruz 1:500-1000), α -integrin β 1 (12G10, ab30394, Abcam 1:200-500), α -ABL2 (M09, clone 5C6, Abnova 1:500-1000). The following small interference RNAs (siRNAs) were purchased: ON-TARGET plus non-targeting pool (siNT), GAG CCA AAU UUC CUA A (siARG #2) GACCAACUCUGGCUUGUUA ON-TARGET plus human MAP4K4 (siMAP4K4 #10, 11, 12, 13 or pool), ON-TARGET plus human MINK1 pool (siMAP4K6), ON-Target plus human TNIK pool (siMAP4K7) (All GE-Healthcare/Dharmacon). Human Moesin siRNA (sc-35955) and Human Ezrin siRNA (sc-35349) both Santa Cruz biotechnology Inc.

Endothelial cell culture

Human Umbilical Vein Endothelial Cells (HUVECs) were purchased from Lonza or freshly isolated from umbilical cords of healthy donors. Cells were isolated and characterized as previously described (Jaffe et al., 1973). Human pulmonary microvascular endothelial cells (PMVECs) were isolated and cultured from healthy donors, approved by the institutional review board of the VU University Medical Center following principles outlined in the Declaration of Helsinki and consent was given. Isolation and culturing of human pulmonary microvascular endothelial cells (PMVECs) from healthy donor lungs was described by our group previously (Szulcek et al., 2016). HUVECs were cultured in M199 medium supplemented with penicillin 100U/ml and streptomycin 100 μ g/mL, L-glutamine 2 mMol/L (all Biowhittaker/Lonza, Verviers, Belgium), heat-inactivated human serum 10% (Sanquin blood supply, Amsterdam, The Netherlands), heat-inactivated new-born calf serum 10% (Gibco, Grand Island, NY), crude endothelial cell growth factor 150 μ g/mL (prepared from bovine brains) and heparin 5U/mL (Leo pharmaceutical products, Weesp, The Netherlands), cultured at 37°C and 5% CO₂, with a medium change every other day. Cells were used for experiments in passage 1-2.

Transfection with small interfering RNAs

Subconfluent HUVECs (80% confluency) were transfected with 10% NBCS/M199 containing 25nM Dharmafect 1 (Dharmacon/GE-healthcare) and 25nM of siRNA. After 16 hours of transfection, medium was changed to regular culture medium to avoid

toxicity. Experiments were done 72 hours after transfection. Efficiency of transfection was evaluated by western blot analysis or PCR of whole cell lysates

Endothelial barrier function assays

Endothelial barrier function was measured by Electrical Cell-substrate Impedance Sensing (ECIS) or macromolecule passage assay. HUVECs were seeded to immediate confluency on gelatin-coated ECIS arrays (Applied Biophysics, Troy, NY). Culture medium was renewed 24 hours after seeding, while experiments were performed 48 hours after seeding. Before thrombin stimulation, cells were incubated with EBM medium containing 1% Human Serum Albumin (HSA, Sanquin CLP) and the compounds in designated concentrations. After 60-90 minutes of pre-incubation, thrombin was added to the wells in a final concentration of 1U/mL (Sigma Aldrich). HUVECs were transfected 24 hours after seeding using Dharmafect 1 and siRNAs for 16 hours, followed by medium change.

For analyzing cell-adhesion cells were serum starved and pre-incubated with DMSO or bosutinib (1 μ M) for 1 hour in m199 containing 1% HSA after which cells were detached by trypsin and counted. A final number of 10.000 cells per well was seeded on gelatin-coated ECIS arrays and resistance was measured during the adhesion- and growth phase for two hours.

After pre-incubation with DMSO (0.01%) or bosutinib (1 μ M) in 1% HSA for 90 minutes, integrin blocking peptides GRGDNP (AS-62049 AnaSpec) and GRGDSP (AS-22945 AnaSpec) dissolved in 1% HSA were added in increasing concentrations of 0-4mM on primary HUVEC monolayers in ECIS. After 60 minutes a plateau-phase was reached and thrombin 1 U/mL was added. When the concentration of the peptides exceeded 500 μ M the barrier could not recover over time and we therefore used an optimal concentration of 450 μ M in subsequent experiments.

Macromolecular passage

HUVECs were seeded to confluency on top of 0.33cm² gelatin-coated ThinCerts[®] cell culture inserts (Greiner Bio-one) with a pore-size of 3.0 μ m and cultured in EGM-2 medium with a medium change every other day. When a solid barrier was formed, defined as the absence of medium leak, cells were pre-incubated for 1 hour with EBM medium containing 1% HSA and the compounds in designated concentrations.

For stimulation, medium in the upper compartment was replaced by 1% HSA/EBM containing horse radish peroxidase (HRP) 5µg/ml and thrombin 1U/mL or a vehicle control. Also 1% HSA/EBM was added to the lower compartment. Samples were taken from the lower compartment for HRP quantification at several time points.

Cells were transfected 24 hours before transfer to 1% gelatin-coated ThinCerts®. HRP was quantified by measuring absorption after adding tetramethylbenzidine (Upstate/Millipore) and sulfuric acid to stop the reaction.

Kinase Binding Assay

In vitro kinase binding assay was performed by GSK following standard procedures. In short, base reaction buffer was prepared, containing 20 mM Hepes (pH 7.5), 10mM MgCl₂, 1mM EGTA, 0.02% Brij35, 0.02 mg/ml BSA, 0.1mM Na₃VO₄, 2mM DTT and 1% DMSO. The indicated kinase was mixed with substrate solution and compounds were delivered into the kinase reaction mixture by Acoustic technology (Echo550; nanoliter range). To initiate the kinase binding reaction, 33P-ATP was added, incubated for 2 hours at room temperature and reactions were spotted onto P81 ion exchange paper. Kinase activity against 396 kinases was detected by filter-binding method. Thresholds for kinase inhibition of ≥75% at 10nM bosutinib and ≤50% at 10µM imatinib were chosen to select candidate kinases.

Protein analysis

For protein analysis, cells were seeded in 5 or 10 cm² culture wells and possibly transfected as described above. When cells reach confluency they were washed with ice-cold PBS and whole-cell lysates were collected by scraping the cells in 2x concentrated SDS sample buffer. Protein samples were separated on 8 or 12.5% SDS page gels or 4-12% precast gels (Biorad) by electrophoresis and transferred to nitrocellulose membranes. Protein analysis was performed by incubation of the nitrocellulose membranes with the designated antibodies. Bands were visualized with enhanced chemiluminescence (Amersham/GE-healthcare) on a AI600 machine (Amersham/GE-healthcare) and intensity was quantified using ImageQuant TL software (GE-healthcare).

Immunofluorescent imaging of cultured endothelial cells

Cells were seeded on 2cm² and 12mm glass coverslips (Menzel), coated with 1% gelatin and crosslinked with 0.5% glutaraldehyde (Sigma Aldrich). Transfected cells were seeded approximately 24 hours after the start of transfection. Untransfected cells were seeded and grown to confluence in 48 hours with a medium change the day after seeding. Cells were pre-incubated with 1% HSA/M199 for 1 hour with bosutinib (1µM) or DMSO, thrombin was added to the wells in a final concentration of 1U/mL. After 2-15 minutes, cells were fixated with warm (37°C) 4% paraformaldehyde (Sigma Aldrich) and put on ice for 15 minutes. Cells were permeabilized with 0,2% triton X-100 in PBS (Sigma Aldrich) and blocked for 30 minutes with 0.1% HSA. Subsequently, coverslips were stained with primary antibodies (in 0.1% HSA/PBS) for 1-2 hours at room temperature. After washing 3 times, the cells were incubated with FITC or Cy5-labeled secondary antibodies (Anti-rabbit or anti-mouse 1:100 in 0.1% HSA/PBS) and F-actin was visualized using labeled phalloidin (in 0,1% HSA/PBS (Tebu bio)) at room temperature for 1-2 hours. After washing, the cells were incubated with DAPI (Thermo Fisher scientific) at room temperature for 30 minutes. Coverslips were mounted with Mowiol4-88/DABCO solution (Calbiochem, Sigma Aldrich). Confocal scanning microscopy was performed on a Nikon A2R confocal microscope (Nikon). Images were analyzed and processed using ImageJ. Gap area was quantified using the freehand selection tool in VE-cadherin staining. The density and number of focal adhesions in total and at the periphery relative to the cell were quantified using ImageJ. In short, images were converted to 8-bit grayscale, foreground/background colors were inverted, and threshold-adjusted. The analyze particles function was used to select and measure focal adhesions. FA were considered peripheral when present at >2/3 of the distance from nucleus to cell membrane. Number of FA was counted and corrected for the number of nuclei. VE-cadherin intensity was quantified using line-measurement from cytosol to cell membrane using ImageJ. Individual peak intensity was divided by individual cytosolic intensity from four positions per pictures, five pictures per condition and averaged in four separate experiments.

Live fluorescence microscopy of FA dynamics

HUVECs were transduced with third generation lentivirus derived from pRRL-Vinculin-GFP plasmid as previously described (Huveneers et al., 2012). Cells were plated in a density of 50,000 cells/mL on Lab-Tek chambered 1.0 borosilicated coverglass slides coated with 3 mg/ml fibronectin. The next day, cells were imaged using Total Internal Reflection Fluorescence (TIRF) microscopy. Immunofluorescent VE-cadherin antibody (BD biosciences 647 anti-human CD144 Cat: 561567) was added 30 minutes before imaging in movie 3 to illustrate cell responses in a monolayer. After 60-90 minutes of DMSO or bosutinib treatment, thrombin was added and imaging continued for 30 minutes with intervals of 30 seconds. Cells were imaged using a NIKON Eclipse TI equipped with a 60x Apo TIRF oil objective (NA 1.49) and an Andor Zyla 4.2 plus sCMOS camera. An Okolab cage incubator and humidified CO₂ gas chamber set to 37°C and 5% CO₂ were used during the imaging process. Original data of single cells without VE-cadherin staining in movie 1&2 was uploaded on the FA analysis server (<http://faas.bme.unc.edu/>) (Berginski et al., 2011, Berginski and Gomez, 2013) for quantification of FA dynamics. Images were enhanced for display with an unsharp mask filter and by adjusting brightness and contrast settings. In brief, FAs were identified based on GFP-vinculin positivity within thresholded images. Dynamic properties ((dis)assembly rate and longevity) of FA was obtained by the tracking of changes in intensity of the fluorescence from single adhesions through subsequent image frames. 9-16 images per condition were imaged and analyzed out of 2 experiments. Please note that in movie 3 the VE-cadherin intensity was equalized and enhanced against bleaching.

MTT cell viability assay

MTT (3-(4,5-dimethylthiazol-2-yl)-2,5-diphenyl-2Htetrazolium bromide) was purchased from Abcam ab211091 lot number GR3285654-2. HUVECs were grown as previously described on 1% gelatin coated 96-wells flat bottom plates in a density of 50,000 cells/well. After 48 hours, cells were incubated with 0, 0.1 μM, 1 μM and 10 μM bosutinib in serum starved medium, or 500 μM H₂O₂ as positive control for 120 min. MTT reagent and MTT solvent were added following manufacturers protocol. Absorbance was read at 590 nm. Percentage cell viability was calculated as (sample-background) / control * 100.

PCR

RNA was isolated and cDNA was generated using RNA-isolation Kit (Zymo Research Direct-zol MiniPrep R2050) and iScript cDNA synthesis kit (Bio-Rad, #170-8891) according to manufacturer's instructions. For PCR reactions FAST SYBR Green Master Mix (Thermo Fisher Scientific, 4385612) was used. qPCR was then performed to quantify the expression of MAP4K4, MAP4K5, MAP4K6 and MAP4K7. GAPDH and TBP were used as housekeeping genes to normalize for the amount of total RNA per sample. Gene expression was determined by the LightCycler 480 Instrument II (Roche Applied Science, Penzberg, Germany), and the reactions were prepared using Light Cycler SYBR Green I Master (Roche Applied Science).

MAP4K4_F1	AAGATGTACGGCCACCTCAC	R1	ATTCCGTTTCACCATTGCTC
MAP4K5_F1	GCAGCCAGCAGTTAGATTCC	R1	TCCAGAAAGCCAACACACTG
MAP4K6_F1	GAGAACAGCAAAGGCCAAAG	R1	TGACCACAGAACCCTTCCTC
MAP4K7_F1	TCACCTGCACCAGCATAAAG	R1	TGCCATCCAGTAGGGAGTTC
TBP-c472-01F	AGTTCTGGGATTGTACCGCA		
TBP-c610-01R	TCCTCATGATTACCGCAGCA		

Animals

The Ethical Committee for Animal Experiments of the Academic Medical Center (Amsterdam, The Netherlands) approved all animal protocols (LEICA-132AE) conform to the guidelines from Directive 2010/63/EU of the European Parliament on the protection of animals used for scientific purposes. Experiments were performed in 42 male C57/Bl6 mice with a mean \pm SD bodyweight of 23.5 ± 1.7 gram purchased from Charles River Laboratories (The Netherlands). Animals were handled one week before the experiment to diminish stress activation. Housing took place in a specific-pathogen free facility on a 12/12 hour light/dark cycle and animals were allowed to take food and tap water ad libitum. Animals were randomized into a control group (NaCl n=6), LPS group (n = 9), and LPS + bosutinib group (n=9). For the additional experiment assessing Evan's blue extravasation, each group consisted out of n=6.

Direct lung injury model

At baseline, mice were weighed and labelled, followed by intranasal administration of lipopolysaccharide (LPS; 5 mg/kg, E. Coli, serotype: 0127:B8, Sigma Aldrich, St. Louis, MO, USA) diluted in 50 μ l NaCl 0.9 % (NaCl, Braun, Germany) or 50 μ l NaCl

0.9% (NaCl group) under isoflurane anaesthesia (2–4 %). Concomitantly, mice received either bosutinib (Selleck chemicals s104, 20 mg/kg dissolved in a solution buffer (2% DMSO, 30% PEG, 5% Tween in MQ) or solution buffer only (control and LPS group) in a total volume of 500uL intraperitoneally (i.p.). After six hours, all animals were sacrificed under general anaesthesia (KDA mix: 1.26 mL 100 mg/mL Ketamine (Anesketin, EuroVetAnimal Health B.V., Bladel, The Netherlands) + 0.2 mL 0.5 mg/mL Dexmedetomidine (Pfizer Animal Health, B.V., Capelle a/d IJssel, The Netherlands) + 1mL 0.5 mg/mL Atropine (Pharmachemie, Haarlem, The Netherlands) in 5mL 0.9 % NaCl by exsanguination via the vena cava inferior. Whole blood was collected in a heparin-coated syringe and centrifuged for 10 minutes at 4000 rpm at 4 °C (Eppendorf, microcentrifuge). Plasma was obtained and stored at –80 °C for further analyses. Bronchoalveolar Lavage Fluid (BALF) was obtained from the left lung. The superior and inferior lobe of the right lung were excised for histopathologic examination. The two middle lobes were used for the lung weight / body weight ratio.

Assessment of lung injury

After ligating the hilum of the right lung, the trachea was cannulated and the left lung was washed three times with 0.3mL saline to obtain BALF. BALF was centrifuged for 10 minutes at 2000 rpm at 4 °C (Eppendorf, microcentrifuge) and stored at –80°C for further analyses. The superior and inferior lobe of the right lung were excised, instilled with 4 % paraformaldehyde and embedded in paraffin for histopathological assessment. The two middle lobes were removed and weighed together directly after resection followed by incubation in a 37 °C stove for determination of the dry weight after seven days. Total protein content in BALF was determined using the Lowry method. Total cell counts in BALF were evaluated with the Beckman Coulter (Fullerton, CA, USA). Differential cell counts were performed on cytospin preparations (Shandon CytospinR 4 Cyto centrifuge; Thermo Electron Corporation) and stained with a modified Giemsa stain (DiffQuick, Dade Behring AG, Duedingen, Switzerland). The inflammatory cytokine Interleukin (IL)–6 was assessed in plasma and BALF and tumor necrosis factor (TNF)– α was measured in BALF using a mouse-specific ELISA kit (R&D systems; Minneapolis, MN, USA) according to manufacturer's instructions. Histologic evidence of lung injury was assessed from hematoxylin and eosin-stained lung sections by using an established histopathologic score from 0 (no injury) to 3 (severe injury). This score consists of endothelialitis,

bronchitis, edema formation, interstitial inflammation and hemorrhage which was scored by a blinded pathologist.

Evans blue extravasation

Lung permeability was determined by assessing tissue accrual of Evans blue (EB) (Sigma Chemical Co.) as previously described (Green et al., 1988). Lung injury was induced and treatment administered as described above. After five hours, mice were anesthetized with isoflurane and 200 μ L of 0.5% Evans blue was administered via the penile vein. One hour later, animals were anesthetized as described above and sacrificed through blood collection from the heart. 5 ml of 0.9% NaCl was injected in the inferior vena cava to rinse the circulation. The right lung was collected, snapfrozen in liquid nitrogen and stored at -80°C . The left lung, kidneys and heart were placed in 300 μ L formamide at 55°C to extract the Evan's blue from the tissue. After 48 hours, the organs were placed in an incubator at 90°C for 24 hours to calculate and correct for dry weight. Evans blue concentration in supernatants was quantified by a dual wavelength spectrophotometric method at 620 nm and 740 nm absorbance and corrected for the dry weight.

Neutrophil isolation

Polymorphonuclear neutrophils (PMNs) were isolated from whole-blood derived from healthy donors. All volunteers signed an informed consent, under the rules and legislation in place within the Netherlands and maintained by the Sanquin Medical Ethical Committee. The rules and legislations are based on the Declaration of Helsinki and guidelines for Good Clinical Practice. Whole blood was diluted (1:1) with 5% (v/v) TNC in PBS. Diluted whole blood was pipetted carefully onto 12.5 ml Percoll (room temperature) 1.076 g/ml. Tubes were centrifuged (Rotanta 96R) at 800G, slow start, low brake for 20 min. Bottom fraction containing PMNs was further processed by erythrocyte lysis in ice-cold isotonic lysis buffer (155 mM NH_4Cl , 10 mM KHCO_3 , 0.1 mM EDTA, pH7.4 in Milli-Q (Millipore)). PMNs were centrifuged at 500G for five minutes at 4°C and incubated again with lysis buffer for 5 min on ice. After another centrifugation at 500G for 5 min at 4°C , PMNs were washed once with PBS and centrifuged again at 500G for 5 min at 4°C before resuspension in HEPES medium (20 mM HEPES, 132 mM NaCl, 6 mM KCl, 1 mM CaCl_2 , 1 mM MgSO_4 , 1.2 mM K_2HPO_4 , 5 mM glucose (all from Sigma-Aldrich) and 0.4 % (w/v) human serum

albumin (Sanquin Reagents), pH7.4). PMNs count and purity was determined by cell counter (Casy) and cells kept at room temperature for no longer than 4 h before use.

Trans-endothelial migration of neutrophils

Primary lung microvascular endothelial cells (PMVECs) were cultured on fibronectin-coated ibidi slides in a density of 0.5×10^5 per channel (μ -slide VI0.4, ibidi). After 72 hours, cells were stimulated for 4h with 100 ng/mL of LPS (Sigma-Aldrich) and 1 μ M DMSO or bosutinib. Freshly isolated PMNs were suspended in HEPES medium and activated by 30 min incubation at 37°C. Flow channels were connected to a perfusion system and exposed to 0.5 mL/min HEPES medium pH 7.4, shear flow (0.8 dyn/cm²) and 1×10^6 cells/channel heat-activated PMN were injected. Leukocyte-endothelial interactions were recorded for 20 min at 0.2 frames/s by a Zeiss Observer Z1 microscope. All live imaging was performed at 37°C in the presence of 5% CO₂. Transmigrated PMNs were distinguished from those adhering to the apical surface of the endothelium by their transition from bright to phase-dark morphology. Number of transmigrated PMNs was manually quantified using ImageJ.

Statistical analysis

Data are represented as mean \pm SD. Comparison of 2 conditions were tested by student t-test. Comparison of more than 2 conditions were tested by 1-way ANOVA or repeated measures ANOVA. Dunnet's posthoc test was used when conditions were compared to one control, bonferroni posthoc test was used when multiple conditions were compared to multiple conditions unless indicated otherwise. P-values were considered statistically significant if $p < 0.05$. Analysis was performed using Graphpad prism software.

ACKNOWLEDGEMENTS

We thank F. Breijer, M.A.W. Maas and N. Bogunovic for helping with experiments.

CONFLICT OF INTEREST: The authors have declared that no conflict of interest exists.

SOURCES OF FUNDING

This work was supported by the Netherlands Cardiovascular Research Initiative: the Dutch Heart Foundation, Dutch Federation of University Medical Centers, the Netherlands Organization for Health Research and Development, and the Royal Netherlands Academy of Sciences Grant 2012-08 awarded to the Phaedra consortium. JA was funded by Dutch Heart Foundation grant number 2014T064. SH was supported by a NWO VIDI grant ZonMW; 016.156.327

REFERENCES

- ADYSHEV, D. M., DUDEK, S. M., MOLDOBAEVA, N., KIM, K. M., MA, S. F., KASA, A., GARCIA, J. G. & VERIN, A. D. 2013. Ezrin/radixin/moesin proteins differentially regulate endothelial hyperpermeability after thrombin. *Am J Physiol Lung Cell Mol Physiol*, 305, L240-55.
- AMAN, J., PETERS, M. J., WEENINK, C., VAN NIEUW AMERONGEN, G. P. & VONK NOORDEGRAAF, A. 2013. Reversal of vascular leak with imatinib. *Am J Respir Crit Care Med*, 188, 1171-3.
- AMAN, J., VAN BEZU, J., DAMANAFSHAN, A., HUVENEERS, S., ERINGA, E. C., VOGEL, S. M., GROENEVELD, A. B., VONK NOORDEGRAAF, A., VAN HINSBERGH, V. W. & VAN NIEUW AMERONGEN, G. P. 2012. Effective treatment of edema and endothelial barrier dysfunction with imatinib. *Circulation*, 126, 2728-38.
- AMMIRATI, M., BAGLEY, S. W., BHATTACHARYA, S. K., BUCKBINDER, L., CARLO, A. A., CONRAD, R., CORTES, C., DOW, R. L., DOWLING, M. S., EL-KATTAN, A., FORD, K., GUIMARAES, C. R., HEPWORTH, D., JIAO, W., LAPERLE, J., LIU, S., LONDREGAN, A., LORIA, P. M., MATHIOWETZ, A. M., MUNCHHOF, M., ORR, S. T., PETERSEN, D. N., PRICE, D. A., SKOURA, A., SMITH, A. C. & WANG, J. 2015. Discovery of an in Vivo Tool to Establish Proof-of-Concept for MAP4K4-Based Antidiabetic Treatment. *ACS Med Chem Lett*, 6, 1128-33.
- AMSELLEM, V., DRYDEN, N. H., MARTINELLI, R., GAVINS, F., ALMAGRO, L. O., BIRDSEY, G. M., HASKARD, D. O., MASON, J. C., TUROWSKI, P. & RANDI, A. M. 2014. ICAM-2 regulates vascular permeability and N-cadherin localization through ezrin-radixin-moesin (ERM) proteins and Rac-1 signalling. *Cell Commun Signal*, 12, 12.
- BAUMGARTNER, M., SILLMAN, A. L., BLACKWOOD, E. M., SRIVASTAVA, J., MADSON, N., SCHILLING, J. W., WRIGHT, J. H. & BARBER, D. L. 2006. The Nck-interacting kinase phosphorylates ERM proteins for formation of lamellipodium by growth factors. *Proc Natl Acad Sci U S A*, 103, 13391-6.
- BERGINSKI, M. E. & GOMEZ, S. M. 2013. The Focal Adhesion Analysis Server: a web tool for analyzing focal adhesion dynamics. *F1000Res*, 2, 68.
- BERGINSKI, M. E., VITRIOL, E. A., HAHN, K. M. & GOMEZ, S. M. 2011. High-resolution quantification of focal adhesion spatiotemporal dynamics in living cells. *PLoS One*, 6, e22025.
- CARNEIRO, P. J., CLEVELARIO, A. L., PADILHA, G. A., SILVA, J. D., KITOKO, J. Z., OLSEN, P. C., CAPELOZZI, V. L., ROCCO, P. R. & CRUZ, F. F. 2017. Bosutinib Therapy Ameliorates Lung Inflammation and Fibrosis in Experimental Silicosis. *Front Physiol*, 8, 159.
- CHUANG, H. C., WANG, X. & TAN, T. H. 2016. MAP4K Family Kinases in Immunity and Inflammation. *Adv Immunol*, 129, 277-314.
- CORTES, J. E., GAMBACORTI-PASSERINI, C., DEININGER, M. W., MAURO, M. J., CHUAH, C., KIM, D.-W., DYAGIL, I., GLUSHKO, N., MILOJKOVIC, D., COUTRE, P. L., GARCIA-GUTIERREZ, V., REILLY, L., JEYNES-ELLIS, A., LEIP, E., BARDY-BOUXIN, N., HOCHHAUS, A. & BRÜMMENDORF, T. H. Bosutinib Versus Imatinib for Newly Diagnosed Chronic Myeloid Leukemia: Results From the Randomized BFORE Trial. *Journal of Clinical Oncology*, 0, JCO.2017.74.7162.

- DEJANA, E. & GIAMPIETRO, C. 2012. Vascular endothelial-cadherin and vascular stability. *Curr Opin Hematol*, 19, 218-23.
- FEHON, R. G., MCCLATCHEY, A. I. & BRETSCHER, A. 2010. Organizing the cell cortex: the role of ERM proteins. *Nat Rev Mol Cell Biol*, 11, 276-87.
- FILEWOD, N. C. & LEE, W. L. 2019. Inflammation without Vascular Leakage Science Fiction No Longer? *American Journal of Respiratory and Critical Care Medicine*, 200, 1472-1476.
- GAVARD, J. 2013. Endothelial permeability and VE-cadherin: a wacky comradeship. *Cell Adh Migr*, 7, 455-61.
- GIANCOTTI, F. G. 2000. Complexity and specificity of integrin signalling. *Nat Cell Biol*, 2, E13-4.
- GORBUNOVA, E. E., GAVRILOVSKAYA, I. N., PEPINI, T. & MACKOW, E. R. 2011. VEGFR2 and Src kinase inhibitors suppress Andes virus-induced endothelial cell permeability. *J Virol*, 85, 2296-303.
- GOVER-PROAKTOR, A., GRANOT, G., PASMNIK-CHOR, M., PASVOLSKY, O., SHAPIRA, S., RAZ, O., RAANANI, P. & LEADER, A. 2018. Bosutinib, dasatinib, imatinib, nilotinib, and ponatinib differentially affect the vascular molecular pathways and functionality of human endothelial cells. *Leuk Lymphoma*, 1-11.
- GREEN, T. P., E., J. D., MARCHESSAULT, R. P. & GATTO, C. W. 1988. Transvascular flux and tissue accrual of Evans blue: effects of endotoxin and histamine. *J Lab Clin Med*, 111, 173-83.
- HAKANPAA, L., KISS, E. A., JACQUEMET, G., MIINALAINEN, I., LERCHE, M., GUZMAN, C., MERVAALA, E., EKLUND, L., IVASKA, J. & SAHARINEN, P. 2018. Targeting beta1-integrin inhibits vascular leakage in endotoxemia. *Proc Natl Acad Sci U S A*.
- HEYEN, J. R., HU, W., JAMIESON, J., THIBAUT, S., BATUGO, M., LOI, C.-M., BURNS-NAAS, L. A., MCHARG, A. D. & JESSEN, B. 2013. Cardiovascular differentiation of imatinib and bosutinib in the rat. *International Journal of Hematology*, 98, 597-607.
- HUANG, C., JACOBSON, K. & SCHALLER, M. D. 2004. MAP kinases and cell migration. *J Cell Sci*, 117, 4619-28.
- HUANG, H., TANG, Q., CHU, H., JIANG, J., ZHANG, H., HAO, W. & WEI, X. 2014. MAP4K4 deletion inhibits proliferation and activation of CD4(+) T cell and promotes T regulatory cell generation in vitro. *Cell Immunol*, 289, 15-20.
- HUVENEERS, S., OLDENBURG, J., SPANJAARD, E., VAN DER KROGT, G., GRIGORIEV, I., AKHMANOVA, A., REHMANN, H. & DE ROOIJ, J. 2012. Vinculin associates with endothelial VE-cadherin junctions to control force-dependent remodeling. *J Cell Biol*, 196, 641-52.
- HYNES, R. O. 2002. Integrins: bidirectional, allosteric signaling machines. *Cell*, 110, 673-87.
- JAFFE, E. A., NACHMAN, R. L., BECKER, C. G. & MINICK, C. R. 1973. Culture of Human Endothelial cells derived from Umbilical veins. *J Clin Invest*, 52, 2745-2756.
- KAPP, T. G., RECHENMACHER, F., NEUBAUER, S., MALTSEV, O. V., CAVALCANTI-ADAM, E. A., ZARKA, R., REUNING, U., NOTNI, J., WESTER, H. J., MAS-MORUNO, C., SPATZ, J., GEIGER, B. & KESSLER, H. 2017. A Comprehensive Evaluation of the Activity and Selectivity Profile of Ligands for RGD-binding Integrins. *Sci Rep*, 7, 39805.

- KHOURY, H. J., CORTES, J. E., KANTARJIAN, H. M., GAMBACORTI-PASSERINI, C., BACCARANI, M., KIM, D. W., ZARITSKEY, A., COUNTOURIOTIS, A., BESSON, N., LEIP, E., KELLY, V. & BRUMMENDORF, T. H. 2012. Bosutinib is active in chronic phase chronic myeloid leukemia after imatinib and dasatinib and/or nilotinib therapy failure. *Blood*, 119, 3403-12.
- KOMAROVA, Y. A., KRUSE, K., MEHTA, D. & MALIK, A. B. 2017. Protein Interactions at Endothelial Junctions and Signaling Mechanisms Regulating Endothelial Permeability. *Circ Res*, 120, 179-206.
- KONG, J. H., KHOURY, H. J., KIM, A. S., HILL, B. G. & KOTA, V. 2017. The safety of Bosutinib for the treatment of chronic myeloid leukemia. *Expert Opin Drug Saf*, 16, 1203-1209.
- LEE, W. L. & SLUTSKY, A. S. 2010. Sepsis and endothelial permeability. *N Engl J Med*, 363, 689-91.
- MACHIDA, N., UMIKAWA, M., TAKEI, K., SAKIMA, N., MYAGMAR, B. E., TAIRA, K., UEZATO, H., OGAWA, Y. & KARIYA, K. 2004. Mitogen-activated protein kinase kinase kinase 4 as a putative effector of Rap2 to activate the c-Jun N-terminal kinase. *J Biol Chem*, 279, 15711-4.
- MATTHAY, M. A., ZEMANS, R. L., ZIMMERMAN, G. A., ARABI, Y. M., BEITLER, J. R., MERCAT, A., HERRIDGE, M., RANDOLPH, A. G. & CALFEE, C. S. 2019. Acute respiratory distress syndrome. *Nat Rev Dis Primers*, 5, 18.
- MEHTA, D. & MALIK, A. B. 2006. Signaling mechanisms regulating endothelial permeability. *Physiol Rev*, 86, 279-367.
- PANNEKOEK, W. J., LINNEMANN, J. R., BROUWER, P. M., BOS, J. L. & REHMANN, H. 2013. Rap1 and Rap2 antagonistically control endothelial barrier resistance. *PLoS One*, 8, e57903.
- PULOUS, F. E., GRIMSLEY-MYERS, C. M., KANSAL, S., KOWALCZYK, A. P. & PETRICH, B. G. 2019. Talin-Dependent Integrin Activation Regulates VE-Cadherin Localization and Endothelial Cell Barrier Function. *Circ Res*.
- PULOUS, F. E. & PETRICH, B. G. 2019. Integrin-dependent regulation of the endothelial barrier. *Tissue Barriers*, 7, 1685844.
- RIZZO, A. N., AMAN, J., VAN NIEUW AMERONGEN, G. P. & DUDEK, S. M. 2015. Targeting Abl kinases to regulate vascular leak during sepsis and acute respiratory distress syndrome. *Arterioscler Thromb Vasc Biol*, 35, 1071-9.
- ROTH FLACH, R. J., SKOURA, A., MATEVOSSIAN, A., DANAI, L. V., ZHENG, W., CORTES, C., BHATTACHARYA, S. K., AOUADI, M., HAGAN, N., YAWE, J. C., VANGALA, P., MENENDEZ, L. G., COOPER, M. P., FITZGIBBONS, T. P., BUCKBINDER, L. & CZECH, M. P. 2015. Endothelial protein kinase MAP4K4 promotes vascular inflammation and atherosclerosis. *Nat Commun*, 6, 8995.
- SHATTIL, S. J., KIM, C. & GINSBERG, M. H. 2010. The final steps of integrin activation: the end game. *Nat Rev Mol Cell Biol*, 11, 288-300.
- SONG, J., ZHANG, X., BUSCHER, K., WANG, Y., WANG, H., DI RUSSO, J., LI, L., LUTKE-ENKING, S., ZARBOCK, A., STADTMANN, A., STRIEWSKI, P., WIRTH, B., KUZMANOV, I., WIENDL, H., SCHULTE, D., VESTWEBER, D. & SOROKIN, L. 2017. Endothelial Basement Membrane Laminin 511 Contributes to Endothelial Junctional Tightness and Thereby Inhibits Leukocyte Transmigration. *Cell Rep*, 18, 1256-1269.
- SU, G., ATAKILIT, A., LI, J. T., WU, N., BHATTACHARYA, M., ZHU, J., SHIEH, J. E., LI, E., CHEN, R., SUN, S., SU, C. P. & SHEPPARD, D. 2012. Absence of integrin alphavbeta3 enhances vascular leak in mice by inhibiting endothelial cortical actin formation. *Am J Respir Crit Care Med*, 185, 58-66.

- SU, G., HODNETT, M., WU, N., ATAKILIT, A., KOSINSKI, C., GODZICH, M., HUANG, X. Z., KIM, J. K., FRANK, J. A., MATTHAY, M. A., SHEPPARD, D. & PITTET, J. F. 2007. Integrin α v β 5 regulates lung vascular permeability and pulmonary endothelial barrier function. *Am J Respir Cell Mol Biol*, 36, 377-86.
- SZULCEK, R., HAPPE, C. M., ROL, N., FONTIJN, R. D., DICKHOFF, C., HARTEMINK, K. J., GRUNBERG, K., TU, L., TIMENS, W., NOSSENT, G. D., PAUL, M. A., LEYEN, T. A., HORREVOETS, A. J., DE MAN, F. S., GUIGNABERT, C., YU, P. B., VONK-NOORDEGRAAF, A., VAN NIEUW AMERONGEN, G. P. & BOGAARD, H. J. 2016. Delayed Microvascular Shear Adaptation in Pulmonary Arterial Hypertension. Role of Platelet Endothelial Cell Adhesion Molecule-1 Cleavage. *Am J Respir Crit Care Med*, 193, 1410-20.
- TACHIBANA, K., HAGHPARAST, S. M. & MIYAKE, J. 2015. Inhibition of cell adhesion by phosphorylated Ezrin/Radixin/Moesin. *Cell Adh Migr*, 9, 502-12.
- TRIPOLITSIOTI, D., KUMAR, K. S., NEVE, A., MIGLIAVACCA, J., CAPDEVILLE, C., RUSHING, E. J., MA, M., KIJIMA, N., SHARMA, A., PRUSCHY, M., MCCOMB, S., TAYLOR, M. D., GROTZER, M. A. & BAUMGARTNER, M. 2018. MAP4K4 controlled integrin β 1 activation and c-Met endocytosis are associated with invasive behavior of medulloblastoma cells. *Oncotarget*, 9, 23220-23236.
- TUINMAN, P. R., MULLER, M. C., JONGSMA, G., HEGEMAN, M. A. & JUFFERMANS, N. P. 2013. High-dose acetylsalicylic acid is superior to low-dose as well as to clopidogrel in preventing lipopolysaccharide-induced lung injury in mice. *Shock*, 40, 334-8.
- VITORINO, P., YEUNG, S., CROW, A., BAKKE, J., SMYCZEK, T., WEST, K., MCNAMARA, E., EASTHAM-ANDERSON, J., GOULD, S., HARRIS, S. F., NDUBAKU, C. & YE, W. 2015. MAP4K4 regulates integrin-FERM binding to control endothelial cell motility. *Nature*, 519, 425-30.
- WANG, Y., JIN, G., MIAO, H., LI, J. Y., USAMI, S. & CHIEN, S. 2006. Integrins regulate VE-cadherin and catenins: dependence of this regulation on Src, but not on Ras. *Proc Natl Acad Sci U S A*, 103, 1774-9.
- WESSEL, F., WINDERLICH, M., HOLM, M., FRYE, M., RIVERA-GALDOS, R., VOCKEL, M., LINNEPE, R., IPE, U., STADTMANN, A., ZARBOCK, A., NOTTEBAUM, A. F. & VESTWEBER, D. 2014. Leukocyte extravasation and vascular permeability are each controlled in vivo by different tyrosine residues of VE-cadherin. *Nat Immunol*, 15, 223-30.
- YAMAMOTO, H., EHLING, M., KATO, K., KANAI, K., VAN LESSEN, M., FRYE, M., ZEUSCHNER, D., NAKAYAMA, M., VESTWEBER, D. & ADAMS, R. H. 2015. Integrin β 1 controls VE-cadherin localization and blood vessel stability. *Nat Commun*, 6, 6429.
- YUE, J., XIE, M., GOU, X., LEE, P., SCHNEIDER, M. D. & WU, X. 2014. Microtubules regulate focal adhesion dynamics through MAP4K4. *Dev Cell*, 31, 572-85.

Figures

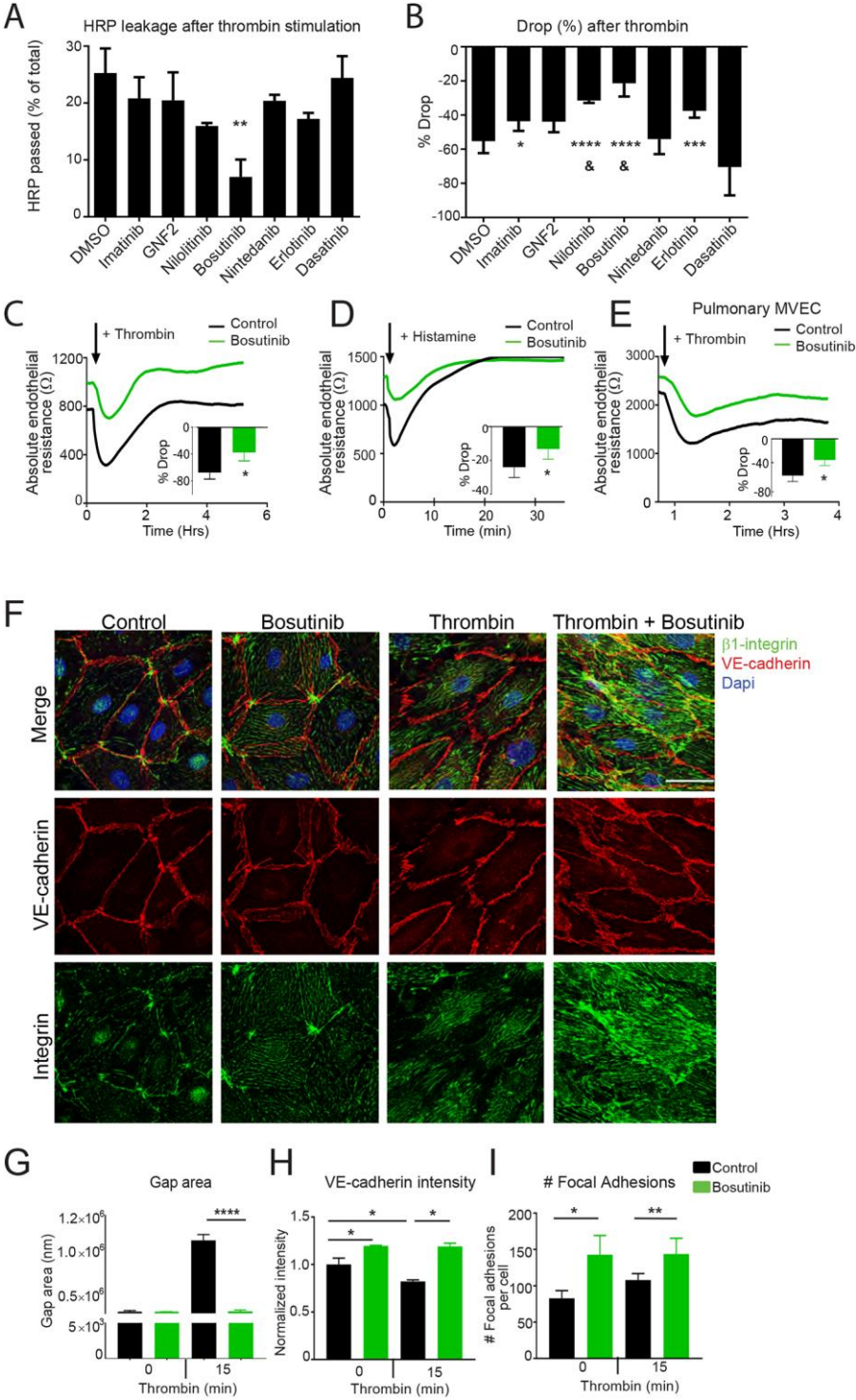


Figure 1 – Bosutinib provides robust protection against inflammation-induced endothelial barrier dysfunction

A) Macromolecule passage over HUVEC monolayers after 2 hours of thrombin stimulation with second and third generation tyrosine kinase inhibitors in their optimal concentration

(n=5-6). Imatinib 10 μ M, GNF2 10 μ M, Nilotinib 10 μ M, Bosutinib 1 μ M, Nintedanib 1 μ M, Erlotinib 10 μ M and Dasatinib 0.1 μ M. B) Quantification of the thrombin response by calculating the maximal drop in endothelial resistance (%) as measured by ECIS. * compared to DMSO control and & compared to imatinib (n=6-8). C-D) Absolute endothelial resistance in HUVECs and quantification of the thrombin and histamine response by calculating the maximal drop in resistance (%) (n=3-4). E) Absolute endothelial resistance in PMVECs and quantification of the thrombin response by calculating the maximal drop in resistance (%) (n=3). F) Immunofluorescent staining of active integrin β 1 (green) and VE-cadherin (red) in control versus bosutinib treated PMVECs counterstained with DAPI (blue). Scale bar represents 50 μ m. Representative images of n=3 experiments. G) Gap area in control versus bosutinib treated PMVECs after 15 minutes of thrombin stimulation (n=3). H-I) VE-cadherin intensity (membrane/cytosol ratio) and number of integrin β 1-containing FA in control versus bosutinib treated PMVECs stimulated with thrombin (n=3). *P<0.05, **P<0.01***P<0.001, ****P<0.0001. All data is represented as mean \pm SD. Comparison of 2 conditions was tested by student t-test. Comparison of more than 2 conditions was tested by 1-way ANOVA or repeated measures ANOVA.

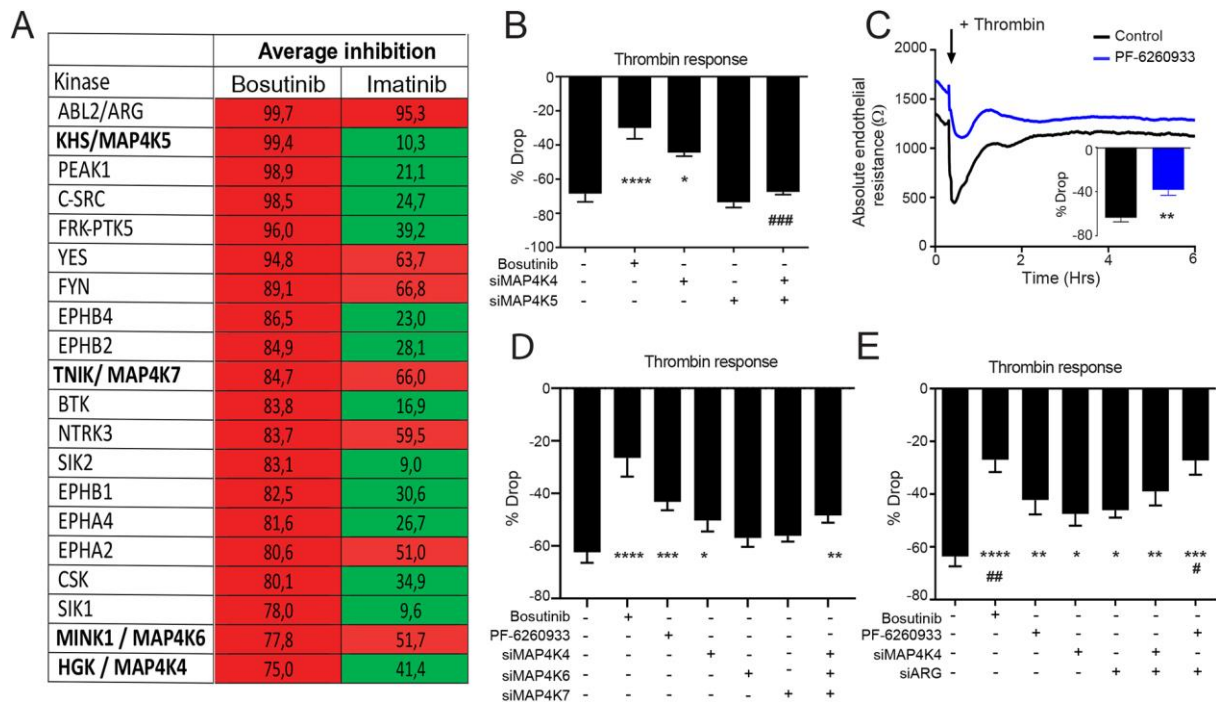
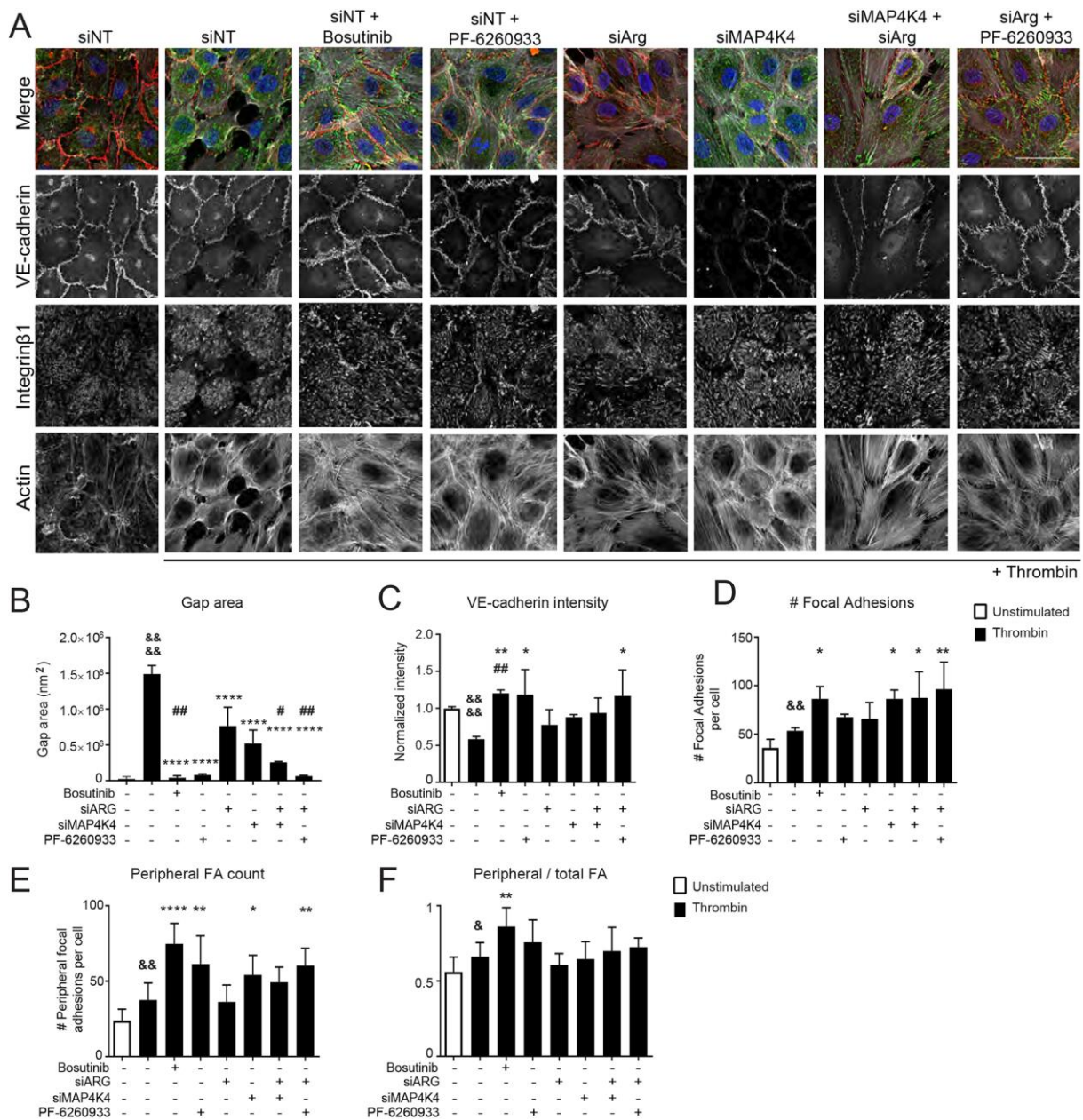


Figure 2 – Inhibition of MAP4K4 by bosutinib enhances endothelial barrier function

A) Comparison of the kinase inhibitory activity of Abl-tyrosine kinase inhibitors bosutinib and imatinib. At a threshold of $\geq 75\%$ inhibition at 10nM bosutinib and $\leq 50\%$ at 10 μ M imatinib 13 kinases were identified to be inhibited by 1 μ M bosutinib but not by 10 μ M imatinib (shown in green), including mitogen-kinase activated family of kinases (MAP4K4/5/6/7). B)

Quantification of the thrombin response by calculating the maximal drop in resistance after siMAP4K4 and siMAP4K5 (%) (n=3-5). C) Absolute endothelial resistance of HUVEC monolayers and percentage drop during thrombin stimulation with 3 μ M pharmacological MAP4K4 inhibitor PF-6260933 (n=3). D) Quantification of the thrombin response by calculating the maximal drop in resistance after bosutinib treatment, PF-6260933 and the knock down of MAP4K4/6/7 (n=3). Quantification of the thrombin response by calculating the maximal drop in resistance after knock down and inhibition of MAP4K4 with knock down of Arg (%) (n=5). *P<0.05 **P<0.01 ***P<0.001 ****P<0.0001 compared to NT control. #P<0.05

###P<0.01 ####P<0.0001 compared to siMAP4K4. All data is represented as mean \pm SD. Comparison of 2 conditions was tested by student t-test. Comparison of more than 2 conditions was tested by 1-way ANOVA.



conditions. #P<0.05 ##P<0.01 compared to siMAP4K4. All data is represented as mean \pm SD. Comparison of 2 conditions was tested by student t-test. Comparison of more than 2 conditions was tested by 1-way ANOVA.

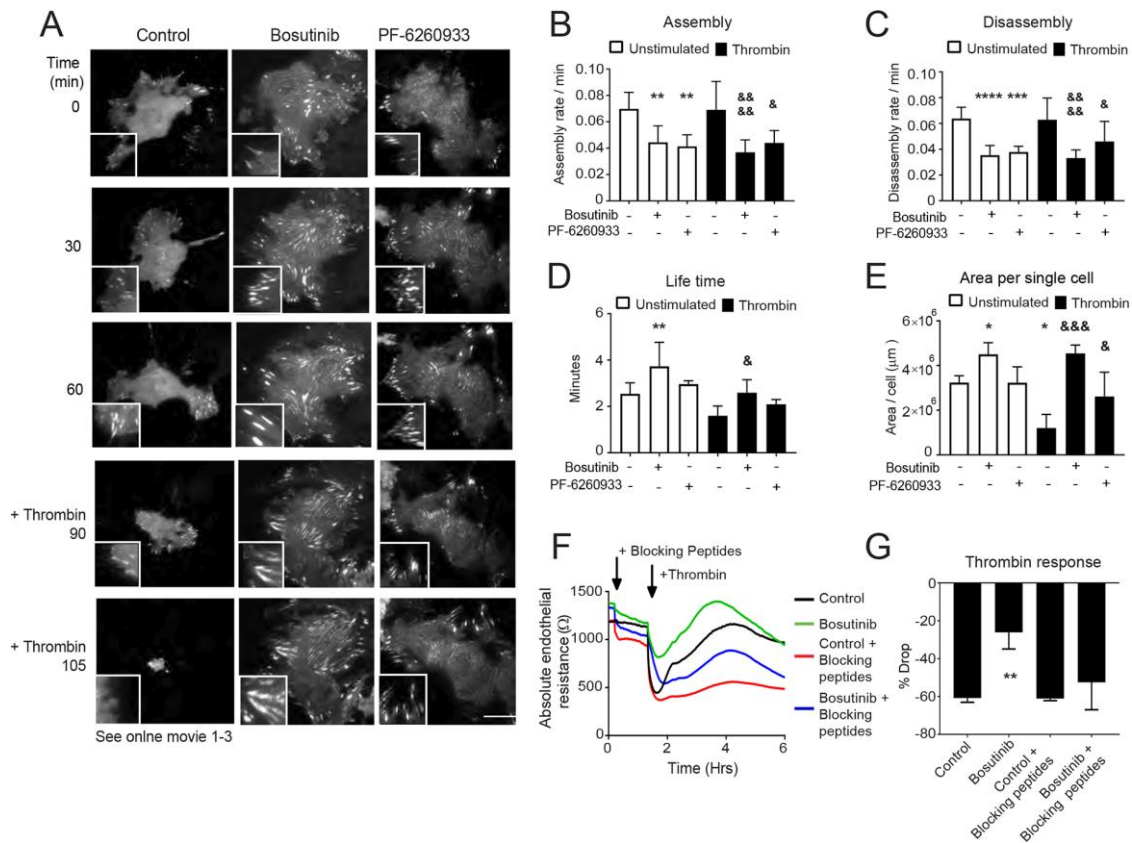


Figure 4 - MAP4K4 enhances FA turnover

A) Representative images of movies on vinculin-containing FA imaged by TIRF microscopy every 30 seconds in control (DMSO), bosutinib or PF-6260933 treatment. Thrombin was added after 90 minutes. Scale bar represents 50 μ m. (B-D) Live-cell imaging analysis of single adhesions, including assembly rate (B), disassembly rate (C) and longevity (D) of GFP-vinculin under control (1 hour imaging) and thrombin stimulated (30-45 minutes imaging) conditions with bosutinib or PF-6260933 treatment (n=9-16 positions in 2 experiments). E) Quantification of single cell area after bosutinib and PF-6260933 under basal conditions and after 90-105 minutes of thrombin stimulation. F) Absolute endothelial resistance of HUVEC monolayers with thrombin stimulation. Control (black), bosutinib treatment (green), control with addition of 450 μ M peptides that block the adhesive function of integrins α v β 5, α 5 β 1 and α v β 3 (red) and bosutinib treatment with addition of 450 μ M peptides that block the adhesive function of integrins α v β 5, α 5 β 1 and α v β 3 (blue) (n=3). G) Quantification of maximal drop in resistance (%) after α v β 5, α 5 β 1 and α v β 3 integrin blocking peptides (n=3) *P<0.05 **P<0.01 ***P<0.001 ****P<0.0001 compared to control. & P<0.05 &&& P<0.01 &&&& P<0.001 compared to thrombin stimulation. All data is represented as mean \pm SD. Comparison of 2 conditions was tested by student t-test. Comparison of more than 2 conditions was tested by 1-way ANOVA.

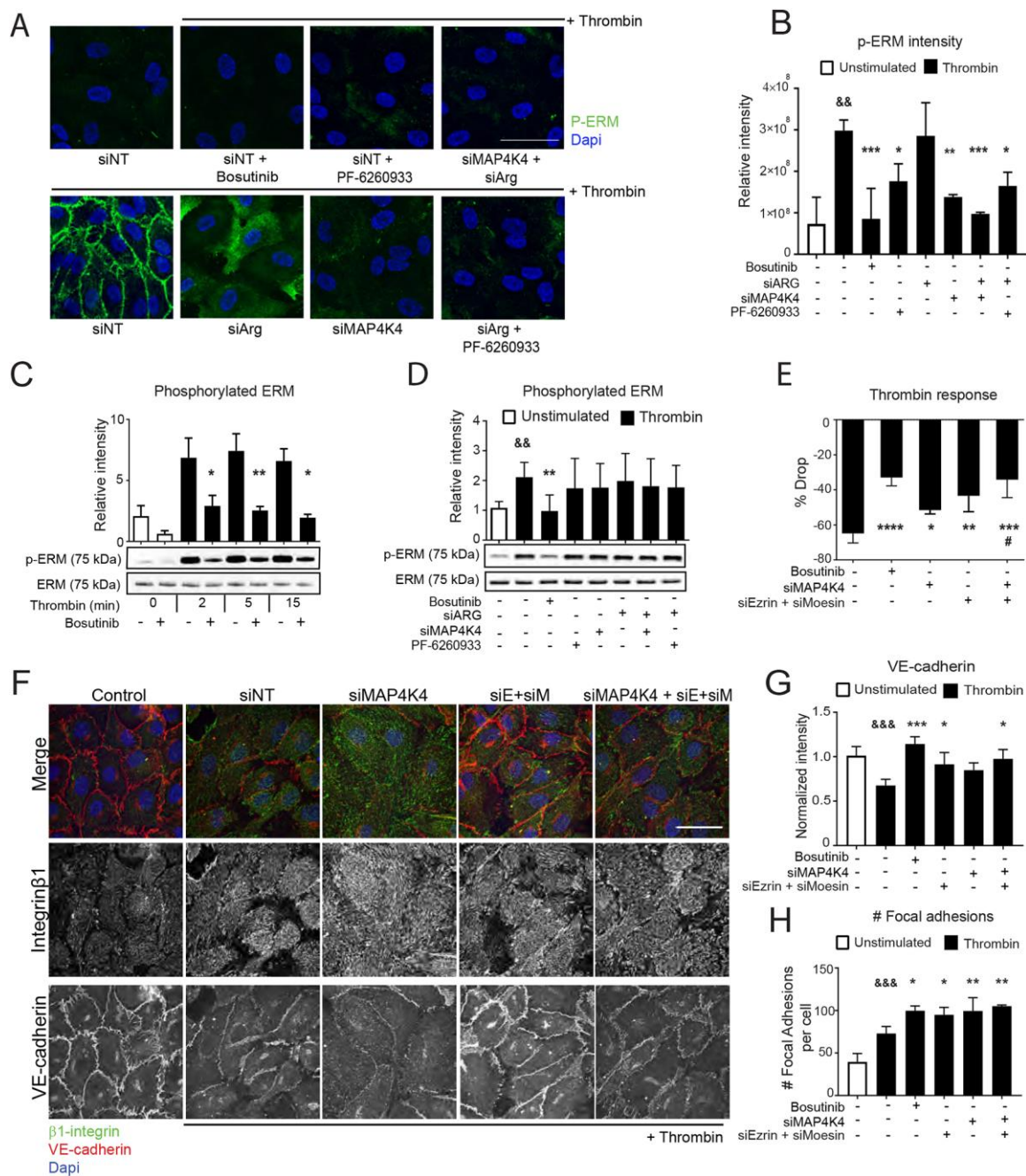


Figure 5 - The MAP4K4-ERM pathway drives FA turnover during endothelial barrier disruption

A) Phospho Ezrin (Thr567)/ Radixin (Thr564)/ Moesin (Thr558) (green) counterstained with dapi (blue) in basal conditions and with 5 minutes of thrombin stimulation in siNT, siNT+bosutinib, siNT+PF-6260933, siARG, siMAP4K4 and siARG+siMAP4K4 or siArg+ PF-6260933 (representative images of n=3) scale bar represents 50µm. B) Quantification of phospho Ezrin (Thr567)/ Radixin (Thr564)/ Moesin (Thr558) intensity in immunofluorescent stainings (n=3). C) Western blot analysis of phospho Ezrin (Thr567)/

Radixin (Thr564)/ Moesin (Thr558) after thrombin stimulation at 0-2-5-15 minutes compared to total ERM (n=3). D) Western blot analysis of phospho Ezrin (Thr567)/ Radixin (Thr564)/ Moesin (Thr558) after thrombin stimulation for 5 minutes compared to total ERM (n=3) E) Quantification of maximal drop in resistance in ECIS (%) after thrombin with bosutinib treatment, siMAP4K4 and PF-6260933 (n=3-4) F) Immunofluorescent staining for active integrin β 1 (green), VE-cadherin (red) and counterstained with DAPI (blue) under basal conditions and with thrombin stimulation for 15 minutes in siNT, siMAP4K4, siE+siM and the combination. Representative images of n=4 experiments, scale bar represents 50 μ m. G) Quantification of VE-cadherin intensity (membrane/cytosol ratio) after 15 minutes of thrombin stimulation (n=3-5). H) Quantification of FA number after 15 minutes of thrombin stimulation (n=4-5). *P<0.05 **P<0.01 ***P>0.001 ****P>0.001 compared to control, &&P<0.01 &&&P<0.001 thrombin response compared to unstimulated condition. # compared to siMAP4K4. All data is represented as mean \pm SD. Comparison of 2 conditions was tested by student t-test. Comparison of more than 2 conditions was tested by 1-way ANOVA.

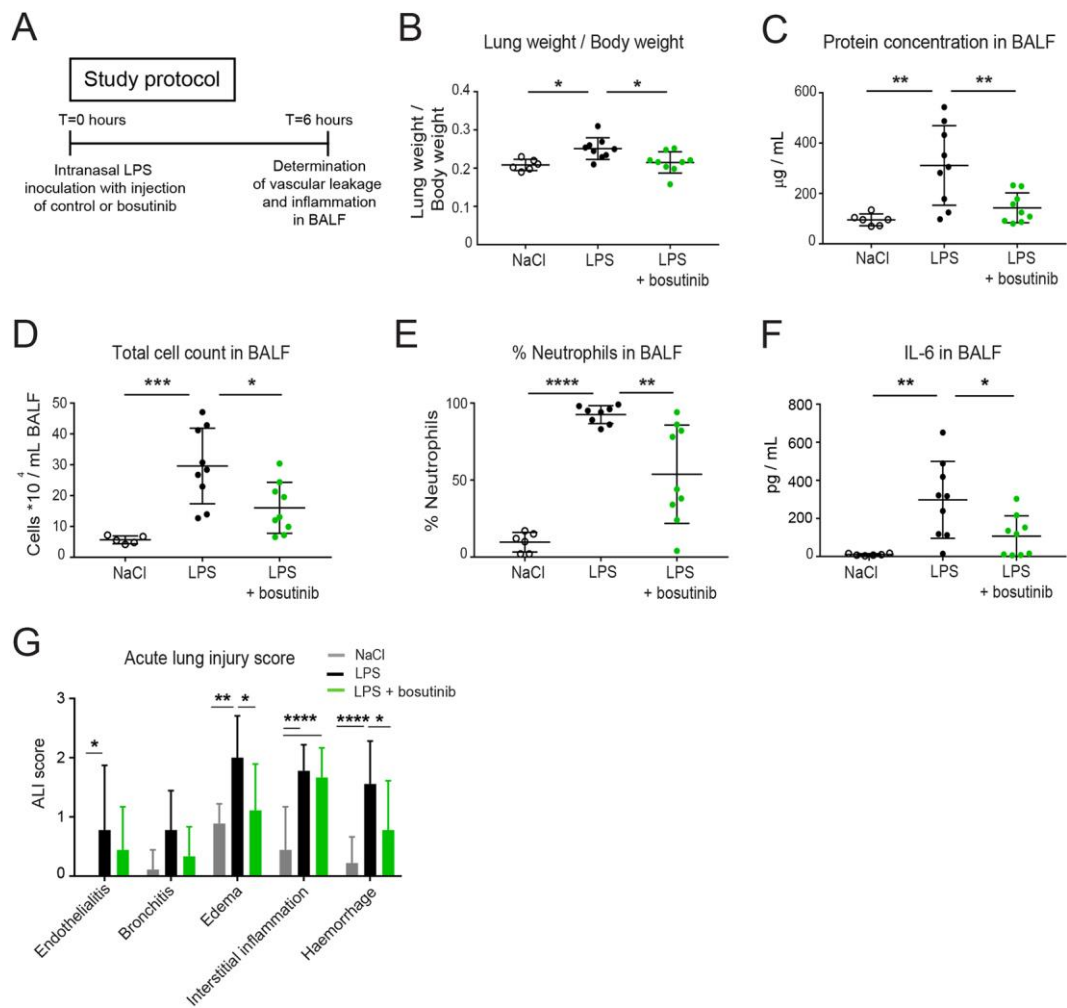


Figure 6 - Bosutinib treatment attenuates LPS-induced pulmonary vascular leakage

A) Lung injury was induced in 42 male C57/BL6J mice by intranasal inoculation of LPS to assess the effect of bosutinib on direct LPS induced lung-injury. B-C) Vascular leakage was determined by calculating the ratio of lung weight divided by the body weight and by measuring protein concentration in BALF (n=6-9 per group). D-F) Inflammation in BALF measured by total cell count, percentage neutrophils and IL-6 concentrations in BALF (n=6-9 per group). G) Acute lung injury score quantified blind in histological coupes of right lungs (n=6-9 per group). *P<0.05 **P<0.01 ***P<0.001 ****P<0.0001. All data is represented as mean \pm SD. Comparison of 2 conditions was tested by student t-test. Comparison of more than 2 conditions was tested by 1-way ANOVA.

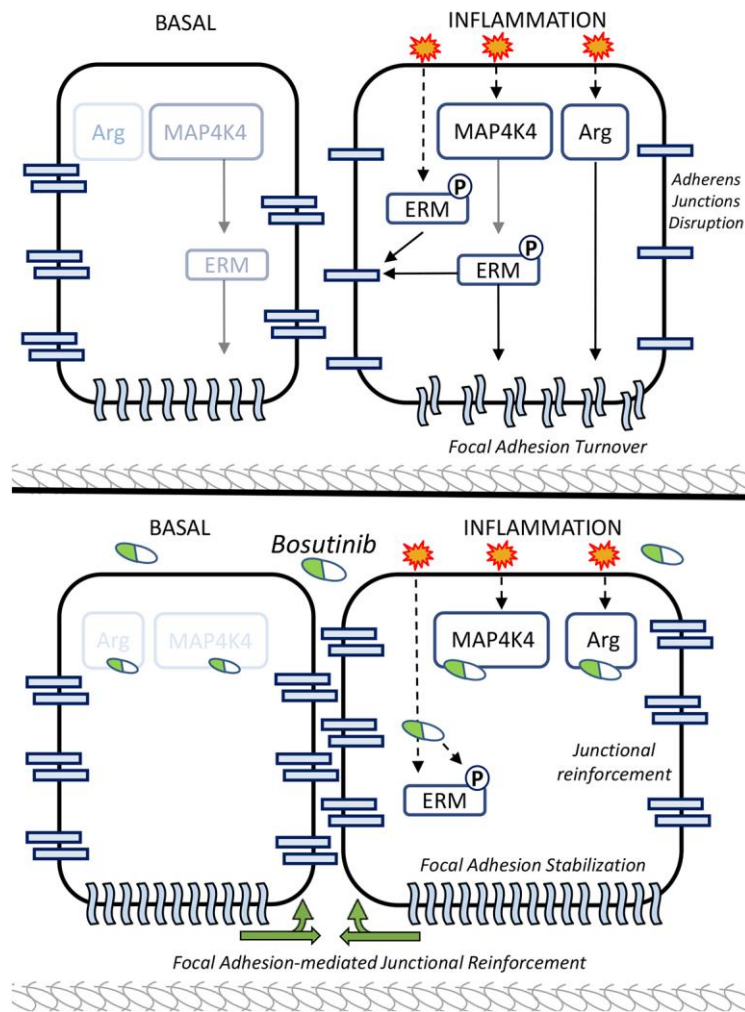


Figure 7 – Proposed mechanism

- A) Under basal conditions, Arg is not active and minor MAP4K4 activity results in minimal FA turnover. During inflammation, for example in thrombin stimulated conditions, MAP4K4 and Arg signal to increase FA turnover, reducing cell-matrix adhesion. MAP4K4 either phosphorylates part of the ERMs at a specific location in the cell and / or affects the translocation of phosphorylated ERM as indicated by a transparent arrow, disrupting AJs.
- B) Bosutinib (indicated as white-green tablet), inhibits several kinases including Arg and MAP4K4, enhancing basal barrier integrity. During inflammation, for example in thrombin stimulated conditions, bosutinib prevents FA turnover through Arg and MAP4K4 inhibition. Bosutinib inhibits ERM activity directly, as through a MAP4K4-inhibiting effect. This results in junctional reinforcement and increased cell-cell contact. Stable FA further signal to AJs, to increase endothelial barrier integrity.

Supplemental Figure 1

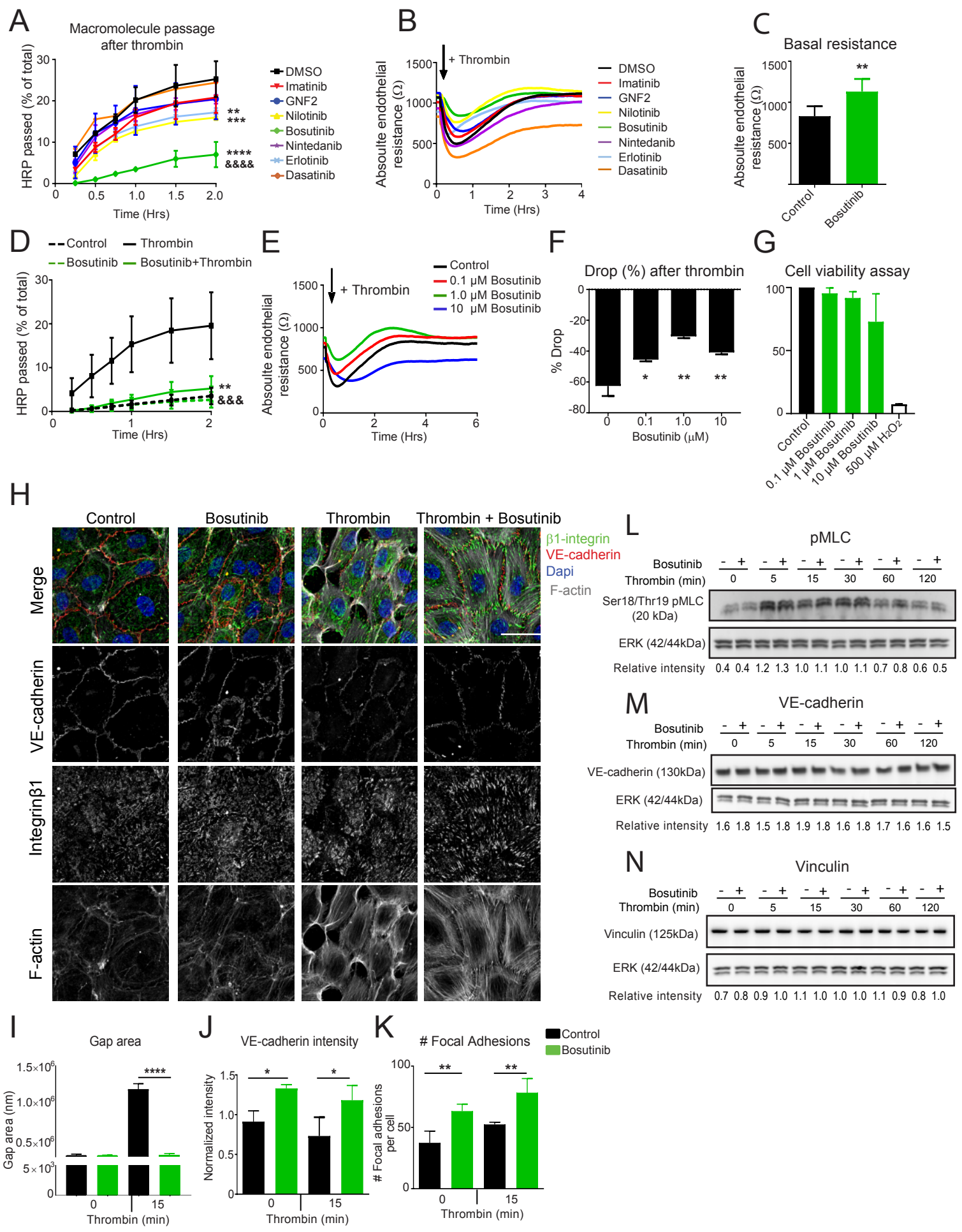


Figure S1

A) Macromolecule passage over HUVEC monolayers after 90 minutes of pre-incubations during thrombin stimulation (n=5-6) with second and third generation tyrosine kinase inhibitors in their optimal concentration (n=5-6). Imatinib 10 μ M, GNF2 10 μ M, Nilotinib 10 μ M, Bosutinib 1 μ M, Nintedanib 1 μ M, Erlotinib 10 μ M and Dasatinib 0.1 μ M B) Absolute endothelial resistance of HUVEC monolayers in ECIS after 90 minutes of pre-incubations with several AKIs (n=3). C) Absolute endothelial resistance of HUVEC monolayers under basal conditions after 90 minutes of bosutinib treatment (n=4). D) HRP passage over HUVEC monolayers with bosutinib compared to control conditions. Dotted line unstimulated condition, continuous line for thrombin treatment (n=3). E) Absolute endothelial resistance of HUVEC monolayers after increasing concentrations of bosutinib incubation (0.1-1.0-10 μ M) and thrombin stimulation (n=3). F) Quantification of the thrombin response (%) by calculating the maximal drop in resistance after increasing concentrations of bosutinib incubation (0.1-1.0-10 μ M) (n=3). G) Cell viability assay as measured by conversion of MTT (3-(4,5-dimethylthiazol-2-yl)-2,5-diphenyltetrazolium bromide). The number of viable cells was measured at an absorbance of OD 590 nm (background corrected) and calculated as OD sample / control * 100. H) Immunofluorescent staining of active integrin β 1 and VE-cadherin and F-actin in control versus bosutinib treated HUVECs counterstained with dapi (blue). Scale bar represents 50 μ m. (Representative images of n=4 experiments). I) Gap area in control versus bosutinib treated HUVECs after 15 minutes of thrombin stimulation (n=4). J-K) VE-cadherin intensity (membrane/cytosol ratio) and number of integrin β 1-containing FA in control versus bosutinib treated HUVECs stimulated with thrombin (n=4) L-N) Western blot analysis of Ser18/Thr19 myosin light chain (MLC) phosphorylation, total VE-cadherin and vinculin after thrombin stimulation (n=3). Representative blots of n=3 *P<0.05 **P<0.01 ***P<0.001 ****P<0.0001 compared to control. &&&P<0.0001 compared to imatinib. &&&P<0.001 compared to thrombin. All data is represented as mean \pm SD. Comparison of 2 conditions was tested by student t-test. Comparison of more than 2 conditions was tested by 1-way ANOVA or repeated measures ANOVA.

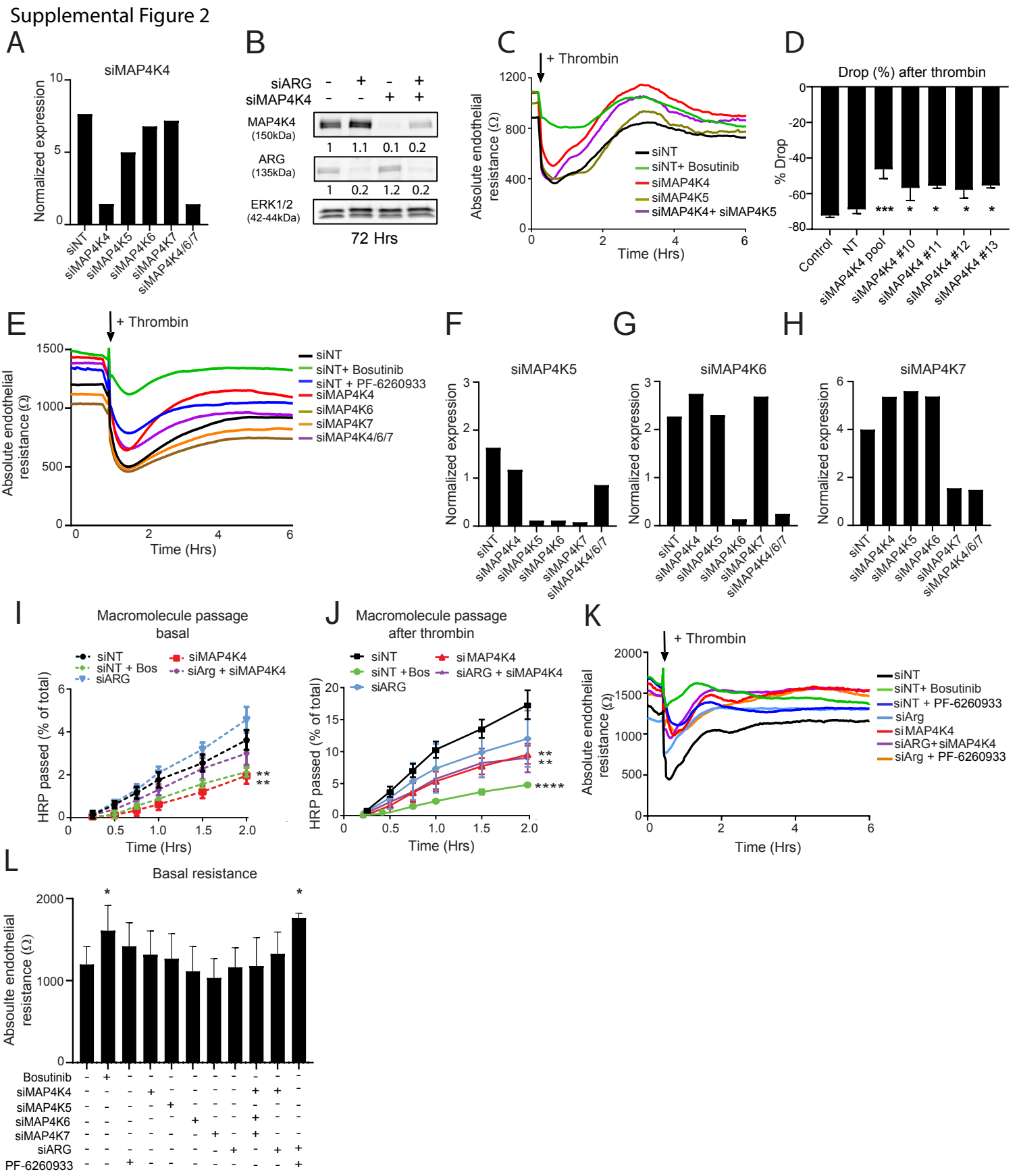


Figure S2

A) mRNA quantity of MAP4K4 measured by qPCR. B) Western blot analysis of Arg and MAP4K4 expression after 72 hours of knockdown. ERK was used as loading control. Representative image of n=3. C) Absolute endothelial resistance of HUVEC monolayers during thrombin stimulation after knockdown of MAP4K4 and MAP4K5 (n=3-5). D) Quantification of the thrombin response by calculating the maximal drop in resistance (%) after different siRNAs for MAP4K4. E) Absolute endothelial resistance in HUVECs after bosutinib treatment, PF-6260933 and knockdown of MAP4K4/6/7 and thrombin stimulation (n=3-4). F-H) mRNA quantity of MAP4K5/6/7 measured by qPCR. I) Macromolecule passage over HUVEC monolayers with siMAP4K4, siArg or the combination or 90 minutes of pre-incubation with bosutinib (n=3-4). J) Macromolecule passage over HUVEC monolayers with siMAP4K4, siArg or the combination or 90 minutes of pre-incubation with bosutinib during 2 hours of thrombin stimulation (n=3-4). K) Absolute endothelial resistance of HUVEC monolayers after bosutinib treatment, PF-6260933 and knockdown of MAP4K4 and Arg and thrombin stimulation (n=4-5). L) Absolute endothelial resistance of HUVEC monolayers under basal conditions with bosutinib treatment, PF-6260933 and knockdown of MAP4K4/5/6/7 or Arg (n=4) *P<0.05 **P<0.01 ***P<0.001 ****P<0.0001 compared to siNT. All data is represented as mean \pm SD. Comparison of 2 conditions was tested by student t-test. Comparison of more than 2 conditions was tested by 1-way ANOVA

Supplemental Figure 3

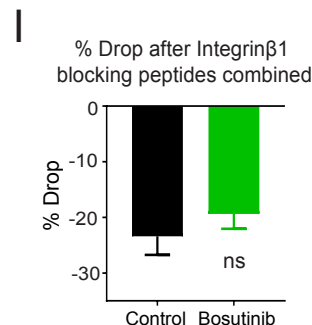
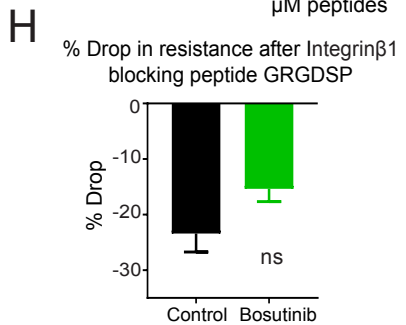
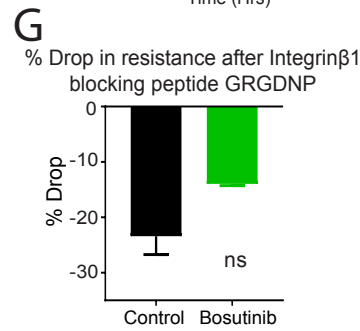
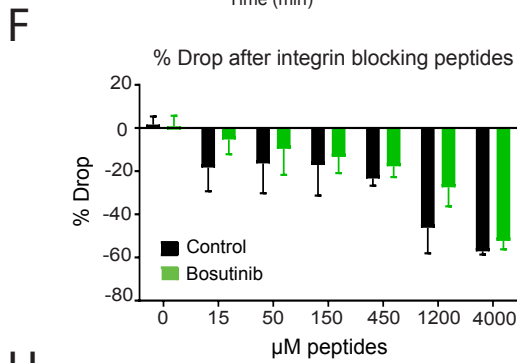
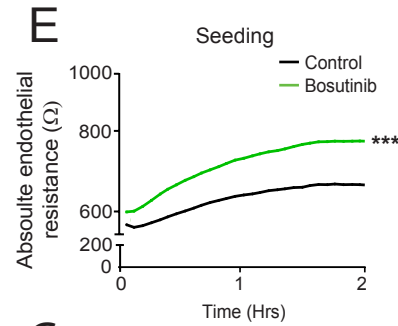
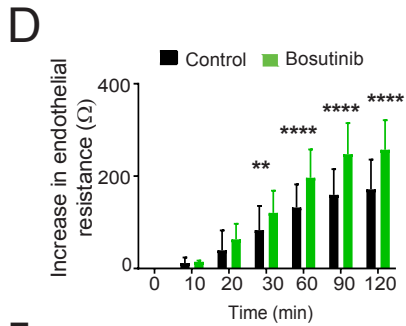
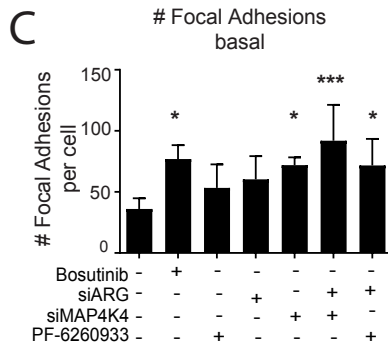
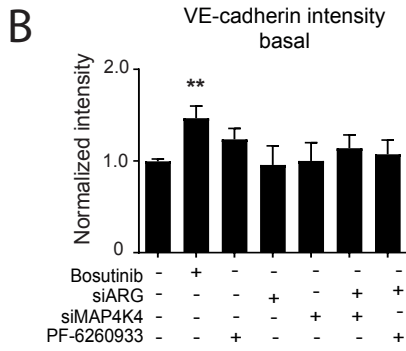
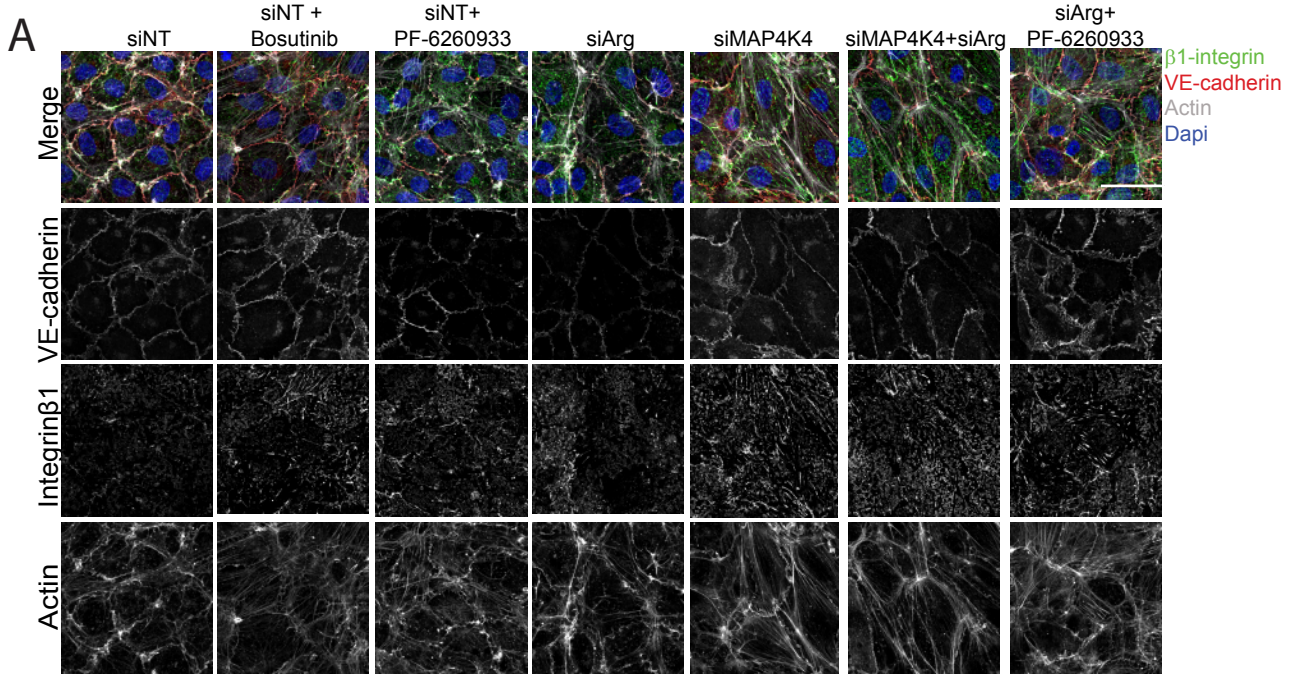


Figure S3

A) Immunofluorescent stainings of active integrin β 1 (green), actin (white) and VE-cadherin (red) under basal conditions and counterstained with dapi (blue). Scale bar represents 50 μ M. (Representative images of n=4 experiments). B) Quantification of VE-cadherin intensity at the membrane divided by the intensity in the cytosol under basal conditions (n=4). C) Quantification of number of FA under basal conditions in active integrin β 1 staining (n=4). D) Increase in endothelial barrier resistance at several time points after 90 minutes of bosutinib pre-incubation (n=3) E) Absolute endothelial resistance of HUVEC monolayers during barrier formation directly after seeding after 90 minutes of bosutinib pre-incubation (n=3). F) Quantification of drop in resistance (%) after addition of increasing concentrations GRGDNP and GRGDSP peptides. Concentrations below 450 μ M combined peptides showed no disruptions of the basal barrier, whereas concentrations exceeding 450 μ M did not show recovery of the barrier over time (n=3). G-H) % Drop in endothelial resistance with Integrin β 1 blocking peptide GRGDNP (blocking the adhesive function of integrins $\alpha\beta$ 3 and α 5 β 1) and GRGDSP (blocking the adhesive function of integrins $\alpha\beta$ 3, $\alpha\beta$ 5 and α 5 β 1) in a total concentration of 450 μ M (n=3). I) % Drop in endothelial resistance after addition of the combined integrin blocking peptides GRGDNP and GRGDSP in a total concentration of 450 μ M (n=3). *P<0.05 **P<0.10 ***P<0.001 ****P<0.0001 compared to control. All data is represented as mean \pm SD. Comparison of 2 conditions was tested by student t-test. Comparison of more than 2 conditions was tested by 1-way ANOVA.

Supplemental Figure 4

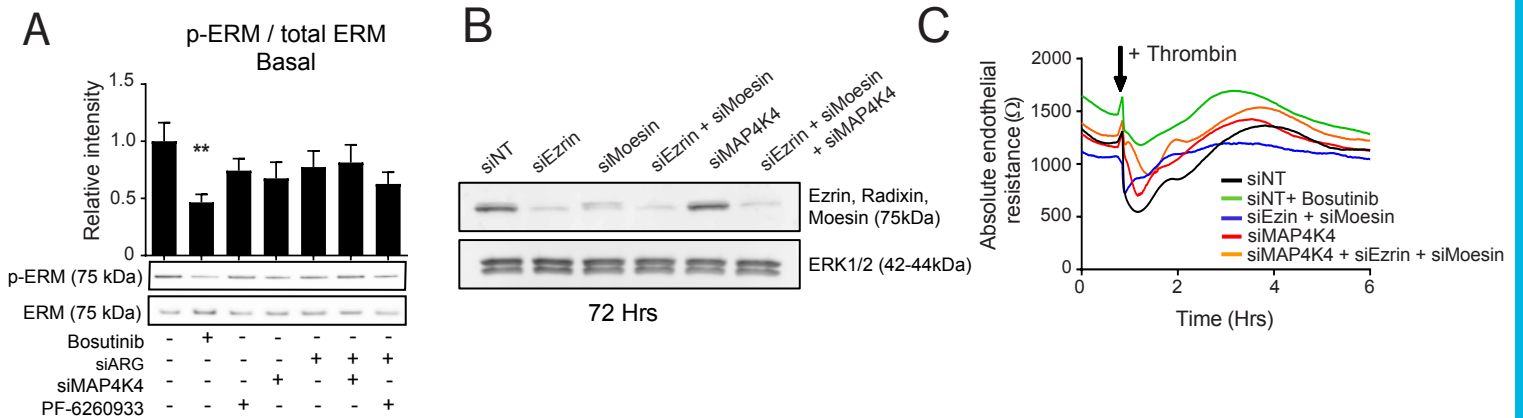


Figure S4

A) Western blot analysis of phosphorylated ERM expression over total ERM expression after bosutinib or PF-6260933 treatment, siMAP4K4, siArg or the combination B) Western blot analysis of ezrin and moesin expression after 72 hours of knockdown. ERK was used as loading control. C) Absolute endothelial resistance of HUVEC monolayers transfected with siMAP4K4 and siEzrin+siMoesin or the combination and stimulated with thrombin (n=4).

Supplemental Figure 5

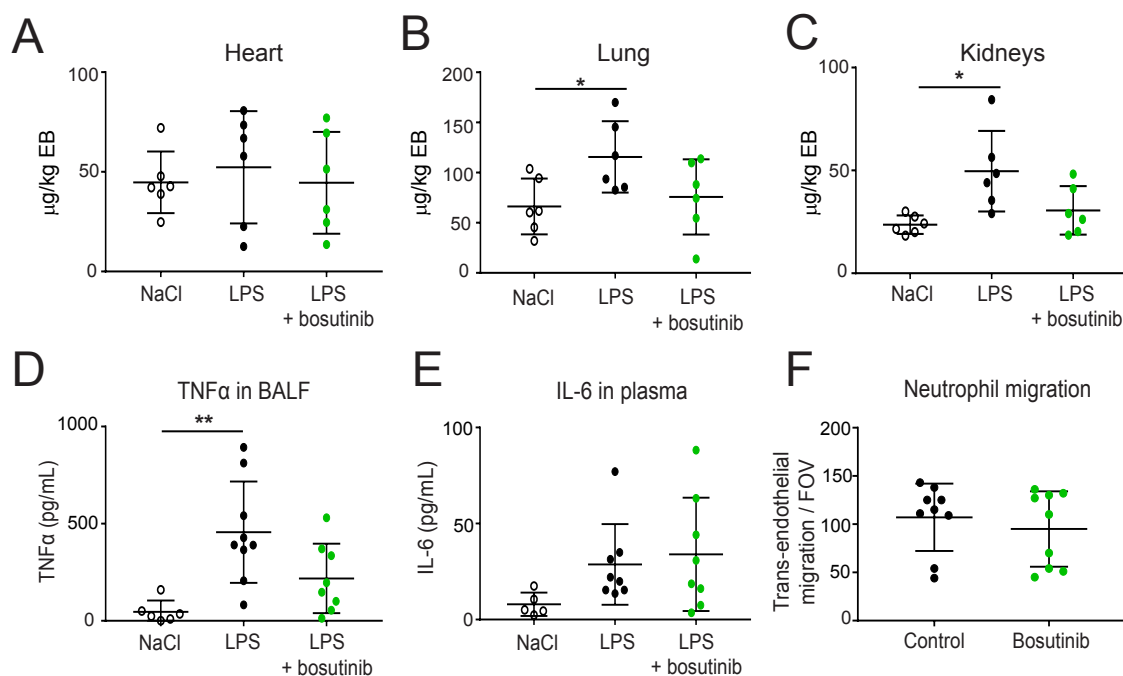
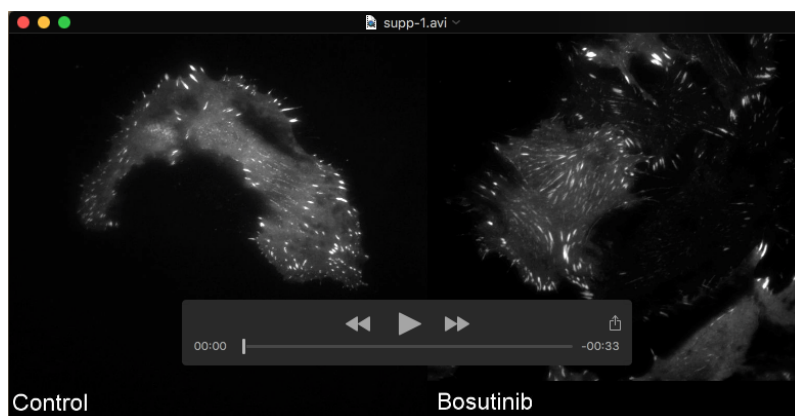
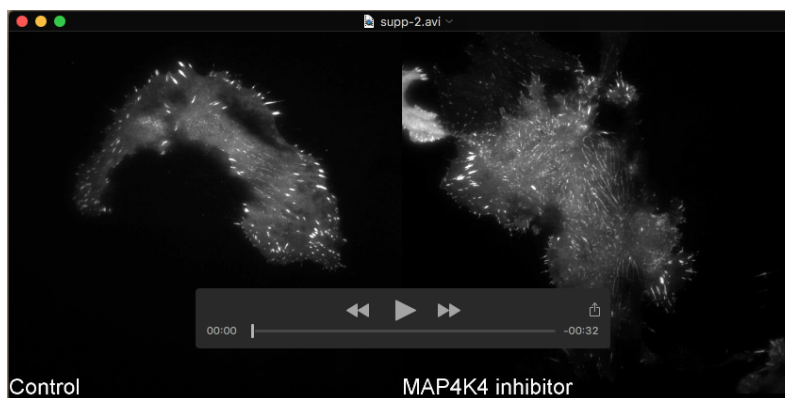


Figure S5

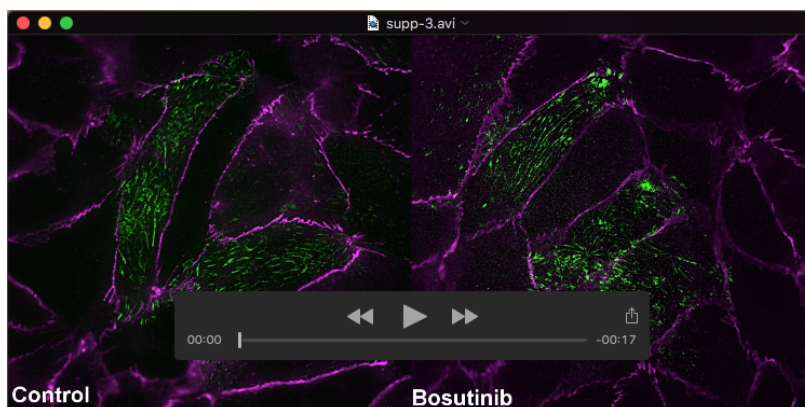
A-C) Vascular leakage of 0.5 % Evans Blue into lungs, kidneys and heart was measured by photospectrometry corrected for Evans Blue in plasma compared between NaCl (control group), LPS and LPS + bosutinib treated mice at T=6 hours (n=6 per group). D) TNFα concentration in BALF (n=6-9 per group). E) IL-6 concentration in plasma (n=6-9 per group). F) Migration of neutrophils over pulmonary microvascular endothelium pre-incubated with or without bosutinib per field of view (FOV). *P<0.05 **P<0.01 compared to NaCl control group. All data is represented as mean ± SD and 1-way ANOVA was used.



Movie 1: Time-lapse confocal imaging of GFP-vinculin in control- or bosutinib-treated HUVEC under basal conditions for 30 minutes, and after thrombin addition 15 minutes. Frame rate 12 frames/s.



Movie 2: Time-lapse confocal imaging of GFP-vinculin in control- or PF-6260933 treated HUVEC under basal conditions 30 minutes, and after thrombin addition 15 minutes. Frame rate 12 frames/s.



Movie 3: Time-lapse confocal imaging of GFP-vinculin with immunofluorescent VE-cadherin in control- or bosutinib treated HUVEC under basal conditions 30 minutes, and after thrombin addition 15 minutes. Frame rate 12 frames/s.